Article

# Controlled Formation of Highly Organized Mesoporous Titania Thin Films: From Mesostructured Hybrids to Mesoporous Nanoanatase TiO

Eduardo L. Crepaldi, Galo J. de A. A. Soler-Illia, David Grosso, Florence Cagnol, Franois Ribot, and Clment Sanchez

*J. Am. Chem. Soc.*, **2003**, 125 (32), 9770-9786• DOI: 10.1021/ja030070g • Publication Date (Web): 17 July 2003



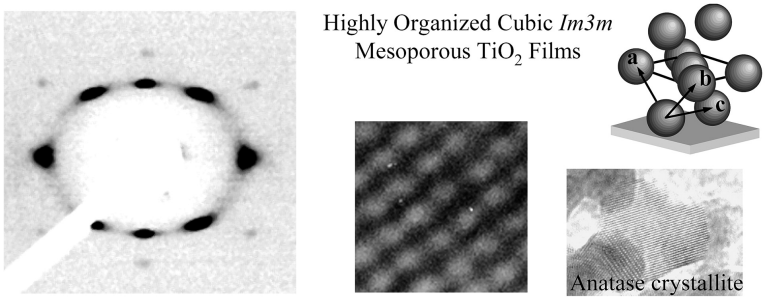


## More About This Article

Additional resources and features associated with this article are available within the HTML version:

- Supporting Information
- Links to the 56 articles that cite this article, as of the time of this article download
- Access to high resolution figures
- Links to articles and content related to this article
- Copyright permission to reproduce figures and/or text from this article

View the Full Text HTML

J|A|C|S
ARTICLES
Published on Web 07/17/2003

# Controlled Formation of Highly Organized Mesoporous Titania Thin Films: From Mesostructured Hybrids to Mesoporous Nanoanatase $TiO_2$

Eduardo L. Crepaldi,[†] Galo J. de A. A. Soler-Illia,[‡] David Grosso, Florence Cagnol, François Ribot, and Clément Sanchez*

*Contribution from the Laboratoire de Chimie de la Matière Condensée, Université Pierre et Marie Curie - CNRS UMR 7574, 4 place Jussieu, 75252 Paris CEDEX 05, France*

Received January 31, 2003; E-mail: clems@ccr.jussieu.fr

***Abstract:*** In this paper, we report the complete synthesis and characterization procedures to generate highly organized and oriented mesoporous titania thin films, using poly(ethylene oxide) (PEO)-based templates. Controlled conditions in the deposition, postsynthesis, and thermal treatment steps allow one to tailor the final mesostructure (2D hexagonal, *p*6*m*, or 3D cubic, *Im*3*m*). Various techniques were used to determine the time evolution of the mesostructure. Spectroscopic techniques (UV/vis, $^{17}O$ NMR) and EXAFS/XANES have been used to follow the chemical changes in the Ti(IV) environment. Crossing these techniques spanning all ranges permits a complete description of the chemistry all the way from solution to the mesostructured metal oxide. A critical discussion on all important chemical and processing parameters is provided; the understanding of these features is essential for a rational design and the reproducible construction of mesoporous materials.

## Introduction

The template approach to mesostructured materials introduced by scientists of the Mobil Co. in the early 1990s[1] opened a land of opportunity for the materials chemistry community. The possibility of designing materials displaying a periodic array of mesopores of tailored and narrowly distributed size promptly attracted the attention of many research groups who explored many different synthesis strategies. The initial approach, based on silica condensation under basic conditions in the presence of alkyltrimethylammonium surfactants as the supramolecular template, applied for the synthesis of the M41S family [MCM-41 (2D-hexagonal, *p*6*m*), MCM-48 (bicontinuous cubic, *Ia*3*d*), and MCM-50 (lamellar)],[1] was widely extended to a wide range of pH's and temperatures using cationic, anionic, neutral, zwitterionic, bolaamphiphile, gemini, and divalent surfactants and a variety of amphiphilic polymers.[2−7] Many new mesophases were discovered, including SBA,[8,9] HMS,[10] MSU,[11,12] KIT,[13] and FDU[14] families, exhibiting different mesostructural symmetries. The pore size can be tailored from the low end of mesopores (∼20 Å) to more than 200 Å, using different templates and swelling agents. Furthermore, the mechanisms involved in the formation of such mesostructured materials are closer to being understood.[6,15]

The research field of periodically organized mesoporous materials started and is still mainly focused on the synthesis of silica-based solids. In part, it can be attributed to the fact that most of the research groups working with mesoporous materials have their origin in the chemistry of zeolites, and thus are much more familiar with the chemistry of the silicates and aluminosilicates than with that of transition metals (TM).[16] Nevertheless, the main reason lies probably in the less explored and more diverse chemistry of the TM when compared to that of silicon. In contrast to the sol−gel chemistry of silicon, TMs generally

[†] Present address: Rhodia Brasil Ltda. CPP, Físico-Química; Fazenda São Francisco s/no - C.P. 07 13140-000 - Paulínia − SP, Brazil.

[‡] Present address: Unidad de Actividad Química, Comisión Nacional de Energía Atómica, Centro Atómico Constituyentes, Av. Gral Paz 1499, 1650 San Martín, Pcia. de Buenos Aires, Argentina.

(1) (a) Kresge, C. T.; Leonowicz, M. E.; Roth, W. J.; Vartuli, J. C.; Beck, J. S. *Nature* **1992**, *359*, 710. (b) Beck, J. S.; Vartuli, J. C.; Roth, W. J.; Leonowicz, M. E.; Kresge, C. T.; Schmitt, K. D.; Chu, C. T.-W.; Olson, D. H.; Sheppard, E. W.; McCullen, S. B.; Higgins, J. B.; Schlenker, J. L. *J. Am. Chem. Soc.* **1992**, *114*, 10834.
(2) Raman, N. K.; Anderson, M. T.; Brinker, C. J. *Chem. Mater.* **1996**, *8*, 1682.
(3) Sayari, A.; Liu, P. *Microporous Mater.* **1997**, *12*, 149.
(4) Barton, T. J.; Bull, L. M.; Klemperer, W. G.; Loy, D. A.; McEnaney, B.; Misono, M.; Monson, P. A.; Pez, G.; Scherer, G. W.; Vartuli, J. C.; Yaghi, O. M. *Chem. Mater.* **1999**, *11*, 2633.
(5) Ying, J. Y.; Mehnert, C. P.; Wong, M. S. *Angew. Chem., Int. Ed.* **1999**, *38*, 57.
(6) Soler-Illia, G. J. de A. A.; Sanchez, C.; Lebeau, B.; Patarin, J. *Chem. Rev.* **2002**, *102*, 4093.
(7) Soler-Illia, G. J. A. A.; Crepaldi, E. L.; Grosso, D.; Sanchez, C. *Curr. Opin. Colloid Interface Sci.* **2003**, in press.
(8) Huo, Q.; Margolese, D. I.; Ciesla, U.; Demuth, D. G.; Feng, P.; Gier, T. E.; Sieger, P.; Firouzi, A.; Chmelka, B. F.; Schüth, F.; Stucky, G. D. *Chem. Mater.* **1994**, *6*, 1176.
(9) (a) Zhao, D.; Feng, J.; Huo, Q.; Melosh, N.; Fredrickson, G. H.; Chmelka, B. F.; Stucky, G. D. *Science* **1998**, *279*, 548. (b) Zhao, D.; Huo, Q.; Feng, J.; Chmelka, B. F.; Stucky, G. D. *J. Am. Chem. Soc.* **1998**, *120*, 6024.
(10) Tanev, P. T.; Pinnavaia, T. J. *Science* **1995**, *267*, 865.
(11) Bagshaw, S. A.; Prouzet, E.; Pinnavaia, T. J. *Science* **1995**, *269*, 1242.
(12) Kim, S. S.; Zheng, W.; Pinnavaia, T. J. *Science* **1998**, *282*, 1302.
(13) Ryoo, R.; Kim, J. M.; Shin, C. H.; Lee, J. Y. *Stud. Surf. Sci. Catal.* **1996**, *105A*, 45.
(14) (a) Yu, C.; Yu, Y.; Zhao, D. *Chem. Commun.* **2000**, 575. (b) Yu, C.; Yu, Y.; Miao, L.; Zhao, D. *Microporous Mesoporous Mater.* **2001**, *44*−*45*, 65.
(15) Patarin, J.; Lebeau, B.; Zana, R. *Curr. Opin. Colloid Interface Sci.* **2002**, *7*, 107.
(16) Schüth, F. *Chem. Mater.* **2001**, *13*, 3184.


**10.1021/ja030070g CCC: $25.00** 

(1) present high reactivity toward hydrolysis and condensation, (2) tend to form closo objects instead of the fractal objects that can be obtained with silica, (3) present different oxidation states and coordination, and (4) present oxides that when heated tend to crystallize. Therefore, the association between TM sol−gel chemistry and the template approach was more difficult to master. Also, the relatively low thermal stability of the mesoporous structure of transition metal oxides (TMOs, as compared to silica-based materials) is often attributed to the crystallization.[16]

TMO-based mesoporous materials have a wide domain of applications, associated to their electronic and magnetic properties. In particular, high surface area mesoporous $TiO_2$ is a very interesting material, in view of controlled delivery, (photo)-catalysis, energy conversion, membrane, and optical applications.[17] For many of these applications, processing the material as a coating is essential. Mesoporous titania thin films have been extensively investigated,[18] but most of the attempts to prepare such films involved the deposition and sintering of $TiO_2$ nanoparticles, leading to aggregates of particles rather than a continuous inorganic phase exhibiting regular and periodic porosity.

Many different synthesis strategies have been developed to synthesize non-silica mesoporous materials, and frameworks based on transition metal oxides, oxo-phosphates and oxo-sulfates, sulfides, and metals.[16,19] Most of the strategies applied to the synthesis of mesoporous transition metal oxides (TMOs) have as a target the control of indiscriminate hydrolysis and condensation by the use of complexing agents[20] such as glycolate,[21] $\beta$-diketones,[22,23] triethanolamine,[24] and peroxide.[25] However, the latter procedures are based on precipitation methods, which are restricted to the formation of powders.

Among the wide variety of synthesis strategies developed so far, the evaporation-induced self-assembly (EISA)[26] method is one of most promising. In such a process, initially coined by Brinker and co-workers for mesoporous silica films,[27,28] the preferential evaporation of solvent (usually an alcohol) concentrates the initial diluted solution in the nonvolatile surfactant and inorganic species before equilibration with atmosphere. By finely tuning the involved variables, one can synchronize the formation of micelles and their organization in a liquid crystal template with the condensation of the inorganic framework, giving rise to well-defined mesostructured hybrids. The main goal of such an approach lies in the possibility of tailoring the macroscopic shape of the resulting mesoporous silicas as spherical particles,[29] thin and thick films,[28,30−34] fibers, and monoliths.[35]

Stucky and co-workers[36] were the first to extend the EISA route for the preparation of mesoporous transition metal oxide powders (including $TiO_2$, $ZrO_2$, $Al_2O_3$, $SnO_2$, $Nb_2O_5$, $WO_3$, and mixed oxides), with 2D-hexagonal or cubic structure, by using ethanolic solutions of $MCl_n$ (inorganic precursor) and nonionic amphiphilic block copolymers (template). In the first interpretation, a nonhydrolytic condensation path was thought responsible for the formation of the inorganic network. However, in the reported synthesis conditions (the solutions were dispersed on open Petri dishes at 40−60 °C and aged for 1−30 days), this path is overwhelmed by ordinary condensation, water being provided by air moisture and impurities.[15]

Titania-ABC mesostructured hybrids have been synthesized by an EISA-derived method in alkoxide−alcohol−water−HCl mixtures,[37,38] stressing the role of water in the mesoscopic organization. In addition, we first demonstrated that highly organized mesoporous titania,[39] zirconia,[40] and alumina[41] and mesostructured mixed valence vanadium oxide-based[42] thin films can be obtained by EISA-derived methods. In our approach, metal chlorides and metal alkoxides are used as the inorganic source, ethanol is used as the solvent, and poly(ethylene oxide)-based nonionic amphiphilic block copolymers (ABC) are used as the template. Despite the similarities to the method proposed by Stucky and co-workers,[36] in our approach, controlled quantities of water are added in solution. This causes an important hydrolysis of the inorganic moieties, resulting in hydrophilic species, with enhanced interactions with the polar portion of the template.[37,38,43] Moreover, water contributes to increase the polarity of the medium, facilitating template folding. Inorganic polymerization can be readily controlled by an acid (added or generated in situ), which is subsequently eliminated by evaporation. Besides the role of the water added to the initial sol, we have also investigated the role of external conditions during deposition; particularly, the relative humidity of the atmosphere is a parameter of paramount importance, which plays a decisive role in the organization of the system.


(17) Hagfeldt, A.; Grätzel, M. *Chem. Rev.* **1995**, *95*, 45.
(18) Gerfin, T.; Grätzel, M.; Walder, L. *Prog. Inorg. Chem.* **1997**, *44*, 345.
(19) Sayari, A.; Liu, P. *Microporous Mater.* **1997**, *12*, 149.
(20) Sanchez, C.; Livage, J.; Henry, M.; Babonneau, F. *J. Non-Cryst. Solids* **1988**, *100*, 65.
(21) Khushalani, D.; Ozin, G. A.; Kuperman, A. *J. Mater. Chem.* **1999**, *9*, 1491.
(22) Antonelli, D. M.; Ying, J. Y. *Angew. Chem., Int. Ed. Engl.* **1995**, *34*, 2014.
(23) Fröba, M.; Muth, O.; Reller, A. *Solid State Ionics* **1997**, *101−103*, 249.
(24) Cabrera, S.; El Haskouri, J.; Guillem, C.; LaTorre, J.; Beltrán-Porter, A.; Beltrán-Porter, D.; Marcos, M. D.; Amorós, P. *Solid State Sci.* **2000**, *2*, 405.
(25) Trong On, D. *Langmuir* **1999**, *15*, 8561.
(26) Brinker, C. J.; Lu, Y.; Sellinger, A.; Fan, H. *Adv. Mater.* **1999**, *11*, 579.
(27) (a) Yang, H.; Kuperman, A.; Coombs, N.; Mamiche-Afara, S.; Ozin, G. A. *Nature* **1996**, *379*, 703. (b) Yang, H.; Coombs, N.; Dag, O.; Sokolov, I.; Ozin, G. A. *J. Mater. Chem.* **1997**, *7*, 1755.
(28) Lu, Y.; Ganguli, R.; Drewien, C. A.; Anderson, M. T.; Brinker, C. J.; Gong, W.; Guo, Y.; Soyez, H.; Dunn, B.; Huang, M. H.; Zink, J. I. *Nature* **1997**, *389*, 364.
(29) Lu, Y.; Fan, H.; Stump, A.; Ward, T. L.; Reiker, T.; Brinker, C. J. *Nature* **1999**, *398*, 223.
(30) Klotz, M.; Albouy, P.-A.; Ayral, A.; Ménager, C.; Grosso, D.; Van der Lee, A.; Cabuil, V.; Babonneau, F.; Guizard, C. *Chem. Mater.* **2000**, *12*, 1721.
(31) Grosso, D.; Babonneau, F.; Albouy, P.-A.; Amenitsch, H.; Balkenende, A. R.; Brunet-Bruneau A.; Rivory, J. *Chem. Mater.* **2002**, *14*, 931.
(32) Zhao, D.; Yang, P.; Melosh, N.; Feng, J.; Chmelka, B. F.; Stucky, G. D. *Adv. Mater.* **1998**, *10*, 1380.
(33) Grosso, D.; Balkenende, A. R.; Albouy, P.-A.; Ayral, A.; Amenitsch, H.; Babonneau, F. *Chem. Mater.* **2001**, *13*, 1848.
(34) Soler-Illia, G. J. de A. A.; Crepaldi, E. L.; Grosso, D.; Durand, D.; Sanchez, C. *Chem. Commun.* **2002**, 2298.
(35) Melosh, N. A.; Lipic, P.; Bates, F. S.; Wudl, F.; Stucky, G. D.; Fredrickson, G. H.; Chmelka, B. F. *Macromolecules* **1999**, *32*, 4332.
(36) (a) Yang, P.; Zhao, D.; Margolese, D. I.; Chmelka, B. F.; Stucky, G. D. *Nature* **1998**, *395*, 583. (b) Yang, P.; Zhao, D.; Margolese, D. I.; Chmelka, B. F.; Stucky, G. D. *Chem. Mater.* **1999**, *11*, 2813.
(37) Soler-Illia, G. J. de A. A.; Sanchez, C. *New J. Chem.* **2000**, 493.
(38) Soler-Illia, G. J. A. A.; Scolan, E.; Louis, A.; Albouy, P. A.; Sanchez, C. *New J. Chem.* **2001**, *25*, 156.
(39) Grosso, D.; Soler-Illia, G. J. A. A.; Babonneau, F.; Sanchez, C.; Albouy, P.-A.; Brunet-Bruneau, A.; Balkenende, A. R. *Adv. Mater.* **2001**, *13*, 1085.
(40) Crepaldi, E. L.; Soler-Illia, G. J. A. A.; Grosso, D.; Albouy, P.-A.; Sanchez, C. *Chem. Commun.* **2001**, 1582.
(41) Pidol, L.; Grosso, D.; Soler-Illia, G. J. A. A.; Crepaldi, E. L.; Sanchez, C.; Albouy, P.-A.; Amenitsch, H.; Euzen, P. *J. Mater. Chem.* **2002**, *12*, 557.
(42) Crepaldi, E. L.; Grosso, D.; Soler-Illia, G. J. de A. A.; Albouy, P.-A.; Amenitsch, H.; Sanchez, C. *Chem. Mater.* **2002**, *14*, 3316.
(43) Soler-Illia, G. J. A. A.; Louis, A.; Sanchez, C. *Chem. Mater.* **2002**, *14*, 750.

Very recently, Stucky and co-workers[44] showed the formation of highly organized mesoporous titania thin films. In this case, instead of the so-called "nonhydrolytic" initial approach, these authors prepared the films from alkoxide−alcohol−water−HCl mixtures, a method very similar to that proposed by Sanchez and co-workers.[37−39]

In the present work, we investigated the role of each of the experimental variables leading to the formation of highly ordered mesoporous $TiO_2$ films, with special attention to the role of water. The structural evolution related to the evaporation process was investigated by a combination of time-resolved synchrotron-SAXS and interferometry. Chemical information at the molecular level has been obtained by EXAFS, $^{17}O$ NMR, UV, and FTIR spectroscopy, which examine the chemical environment of the metal or oxo ions. Crossing these techniques with mass spectroscopy of vapor fraction and EDS analysis of the film surface, used to follow the evolution of volatile species, leads to a better comprehension of the formation paths. As we shall see, as-prepared coatings are "titanotropic";[43] that is, they behave like hybrid liquid crystals. We observed that one can take advantage of this "flexibility" to control, during the aging process, the organization, the final mesostructure, and the optical quality of the films. A sequence of treatments was developed to convert the mesostructured hybrids in high surface area mesoporous coatings with nanocrystalline framework. Very high thermal stability was achieved, reaching 600 °C for the periodicity. Films with surface area in excess of 100 $m^2\ g^{-1}$, exhibiting a wormlike, 2D-hexagonal, or cubic mesostructure, and anatase as the main component of the inorganic framework, can be reproducibly obtained. A formation mechanism, all the way from the molecular to the nanocrystalline mesoporous material, is also proposed.

## Experimental Section

**Preparation of Initial Solutions.** $TiCl_4$ or $TiCl_4/Ti(OEt)_4$ (Fluka) mixtures were used as the inorganic source. Poly(ethylene oxide)-based nonionic diblock $[C_nH_{2n-1}(OCH_2CH_2)_yOH$, Brij 56 (B56, $n/y = 16/10$) or Brij 58 (B58, $n/y = 16/20$)] or triblock copolymers $[HO(CH_2CH_2O)_n(CH_2CH(CH_3)O)_m(CH_2CH_2O)_nH$, Pluronic P123 (P123, average $n/m = 20/70$) or Pluronic F127 (F127, average $n/m = 106/70$)] were used as structure directing agents. All templates are commercially available from Aldrich.

A typical solution was prepared by the slow addition of the inorganic precursor[45] into an ethanolic solution of the template in the molar ratio $1TiCl_4$:20−80EtOH:*s* template. The parameter *s* was adjusted so that the typical sol contained approximately 1 ethylene oxide (EO) group per metal (e.g., 0.05Brij 58/Ti or 0.005Pluronic F127/Ti); however, a more extended ratio from 0.3 to 4EO/Ti was investigated.[46] To this mixture was slowly added water ($0-20H_2O/Ti = h$). The addition of water causes the hydrolysis of the inorganic moieties, producing in situ ethanol and HCl, the latter being the reason for the high stability of the sols. The final solutions are very acidic ($[H^+] > 1$ mol $dm^{-3}$) and stable for several months at ambient temperature (20−25 °C) or 1−2 weeks at 30 °C.

$$TiCl_4 + 2EtOH \rightarrow TiCl_2(OEt)_2 + 2HCl \quad (1)$$

$$TiCl_2(OEt)_2 \xrightarrow{mH_2O} [Ti(OH)_2(H_2O)_n(Z)_x]^{(2-x)+} + (\sim 2 - x\text{HCl}) + (\sim 2 - x\text{EtOH}); \quad Z = OH, Cl, OEt; \quad m > 4; \quad x < 2 \quad (2)$$

The presence of such chemical species is supported by $^{17}O$ NMR, UV, and EXAFS experiments (vide infra) and previous reports by Bradley.[47]

**Film Preparation.** Films were deposited at temperatures ranging from 20 to 45 °C by dip-coating silicon wafer, fused silica, or glass substrates at constant withdrawal rates between 1 and 5 mm $s^{-1}$. The relative humidity (RH) inside the dip-coater chamber was carefully controlled between 10% and 80%. After the drying process, films were aged at controlled RH and temperature (20−35 °C), between 24 h and 2 weeks. A gradual heating was applied to increase inorganic polymerization and stabilize the mesophase, typically 60, 100, and 130 °C in air (24 h at each temperature). Finally, the template was removed by calcination in air at temperatures between 300 and 800 °C (1 °C $min^{-1}$ ramp) for 6 h.

**Optimal Conditions.** Well-organized $TiO_2$-based crystalline (anatase) cubic *Im*3*m* mesoporous coatings are obtained using the following procedure. The solution is prepared by adding 0.01 mol (1.93 g) of $TiCl_4$ to a solution containing 0.40 mol (18.43 g) of anhydrous ethanol and $5 \times 10^{-5}$ mol (0.67 g) of Pluronic F127 ($s = 0.005$). To this solution, 0.1 mol (1.8 g) of water is slowly added ($h = 10$). Films are prepared by dip-coating silicon wafer or glass substrates at a withdrawal rate of 1.5 mm $s^{-1}$ and RH = 30%. Immediately after the drying line reaches the drop, the RH is raised to 50%. Films are aged at RH in the 50−60% range for at least 2 days (longer aging times give slightly better results, see below), and they are heated at 60, 100, and 130 °C for 24 h at each temperature. Calcination is done in air at 400−600 °C (ramp of 1 °C $min^{-1}$) for 4 h. $TiO_2$ naonocrystalline coatings with 2D hexagonal structures are reproducibly obtained following the same procedures with an *s* ratio of 0.09.

**Characterization.** Low-angle X-ray diffraction (XRD) diagrams were collected in $\theta-2\theta$ mode using a conventional goniometer PW 1820 Philips (Cu $K\alpha_1$ radiation, $\lambda = 1.5406$ Å). Wide-angle XRD patterns were collected in parallel mode ($\omega = 0.5°$, $2\theta$ varied from 10° to 70°, Cu $K\alpha_1$ radiation) using a Philips X'Pert PW-3050 with a thin film optic. The crystallite size was estimated by applying the Scherrer equation to the fwhm of the (101) peak of anatase, with silicon as a standard for the instrumental line broadening. Transmission electron microscopy images in ordinary (TEM) or high (HRTEM) resolution were collected using a JEOL 100 CX II (120 kV) or a Philips CM 20 (200 kV) microscope, respectively. Samples obtained by scratching the films from the substrate were embedded in epoxy resin and ultramicrotomed, or suspended in ethanol. In both cases, carbon-coated copper grids were used as the sample holder. Scanning electronic microscopy (SEM) coupled to EDX investigations (JEOL JSM-5200 Scanning Microscope operating at 20 kV, coupled to an Oxford Link Pentafet 6880 for surface elemental analysis) was performed to evaluate the morphology and the composition of the film surface. FT-IR spectrophotometry was carried out with a Nicolet Magna 500 apparatus, on samples scratched off the substrate and dispersed in KBr pellets. Nitrogen adsorption−desorption isotherms were collected at −196 °C using Micromeritics ASAP 2010 equipment (BET and BJH models, respectively, for surface area and porosity evaluation) on samples scratched off the substrate.

In situ evaluation of the structural evolution of films during dip-coating has been performed in transmission mode using the synchrotron

(44) Alberius, P. C. A.; Frindell, K. L.; Hayward, R. C.; Kramer, E. J.; Stucky, G. D.; Chmelka, B. F. *Chem. Mater.* **2002**, *14*, 3284.

(45) The inorganic precursors are quickly hydrolyzed and must be manipulated in inert, dry atmosphere. Care must be taken during the addition of $TiCl_4$ into the template alcoholic solution, because the reaction is exothermic and HCl is released.

(46) Inside this range, the template to $TiO_2$ ratio (w/w) is in the 0.15−3.4 range. The density of the inorganic phase for freshly deposited coatings can be estimated as reported elsewhere,[44] giving rise to a value around 2 g $cm^{-3}$. As such, the template volume fraction ($\Phi T$) can be calculated to be in the 25−90% range, the limits depending on the ABC and *s*. For a typical F127 solution, with $s = 0.005$, $\Phi T = 62.7\%$, inside the cubic (*Im*3*m*) domain in the F127/water phase diagram; see ref 82.

(47) Bradley, D. C.; Mehrotra, R. C.; Gaur, D. P. *Metal Alkoxides*; Academic Press: London, 1978.

radiation of the small-angle X-ray scattering (SAXS) beam-line (8 keV, $\lambda = 1.54$ Å) of ELETTRA (Trieste, Italy). More details on such an experiment, involving both techniques, have been published elsewhere.[33,41,42,48]

SAXS measurements were also performed at the D43 line of LURE (Orsay, France). For these experiments, films were prepared and aged in different conditions for a complete evaluation of the final mesostructure. Image plates were used as the detector, and long accumulation times (20−60 min) were applied to enhance the signal-to-noise ratio. The evolution of the mesostructure during thermal treatment was investigated from 100 to 800 °C using this apparatus.

Liquid state $^{17}O$ NMR experiments were performed in a Bruker AC300 spectrometer operating at 54.2 MHz. $^{17}O$-enriched water (10% $^{17}O$, Euriso-top, Gif-Sur-Yvette, France) was used to enhance the signal-to-noise ratio.[49] Acquisition conditions were 15 $\mu$s pulse, 0.2 s cycle delay, and 2500 or 1250 scans for 3% or 5% enriched water (diluted from 10% enriched with deionized water), respectively. $H_2O$ was used as the external reference (0 ppm).[50]

X-ray absorption spectroscopy at the titanium K edge has been performed at LURE (Orsay, France). Samples were studied in transmission (solutions) or in total electron yield (films) mode. EXAFS modulations were extracted from the absorption spectra following standard procedures[51−54] and were analyzed according to the single scattering model with backscattering amplitude and phase functions computed from $TiO_2$−anatase[55] or titanium chloroalkoxides[56] with the ab initio code FEFF 7.[57]

The evolution of the volatile species (ethanol, water, and HCl) was followed by mass spectroscopy (MS) using a Hiden HPR-20 benchtop gas analyzer connected to a controlled gas flow system. Signals from EtOH ($m/z^+ = 46$, 31), $H_2O$ ($m/z^+ = 18$), and HCl ($m/z^+ = 36$ and 38) were analyzed; blank experiments using water/EtOH/HCl mixtures were performed to separate the EtOH and $H_2O$ contributions to the different peaks. The evolution of free-water content in the film was estimated from parallel experiments in which 10 g of the initial sol was allowed to evaporate under a constant air flux of controlled RH (e.g., 20%, 40%, and 70%). The weight percent of water was then measured by the Karl Fisher technique using a Metrohm 701 KF Titrino apparatus.

In situ ellipsometry measurements were performed, to assess the film thickness and refractive index and to determine IR absorption during film drying at three different RH values (1%, 40%, and 80%). More details on the experimental setup and on the data analysis for in situ SAXS, EXAFS, MS, and ellipsometry are given as Supporting Information (SI).

## Results and Discussion

**From Solution to Hybrid Mesostructures: Chemical Behavior in the Precursor Solutions.** UV/vis spectroscopy, $^{17}O$ NMR, and XANES/EXAFS have been used to assess the chemical phenomena taking place in the initial solutions; a short global description will be first given here, to settle the context of the discussion. These features have been proven decisive in organization, as will be shown in the following section, dedicated to mesostructure characterization. Upon mixing $TiCl_4$ and ethanol, a marked yellow color is developed; UV−vis measurements (see SI) show an intense band with a maximum at 390−400 nm, due to charge transfer from the $Cl^-$ ligands to the Ti(IV) $d^0$ center. Upon water addition, this band shifts to lower wavelengths and markedly decreases in intensity, reaching a $\lambda_{max} \approx 370$ nm for $h = 10$ (SI), a value higher but relatively similar to the 320−340 nm value previously found.[58] This trend suggests that the initial chloro-alkoxide complex (probably solvated $TiCl_2(EtO)_2$, a well-known major product of $TiCl_4$ alcoholysis)[47] is modified by the addition of water, by either hydrolysis, condensation, or both, which shift the electronic ($\pi_{Cl} \rightarrow t_{2gTi}$) transitions to a higher frequency.

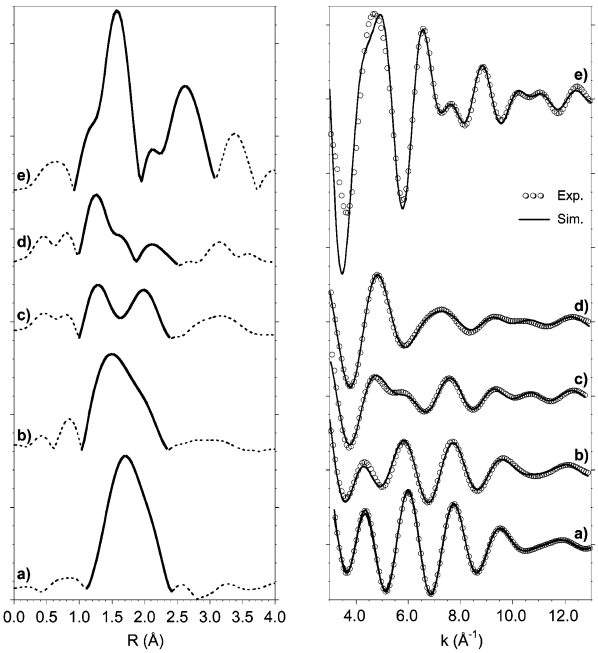


***Figure 1.*** Fourier transforms moduli of the EXAFS signals (the thicker line shows the part of the pseudoradial distribution which was filtered, back Fourier transformed, and simulated) and simulations for (a) a solution made of $TiCl_4 + 40EtOH + 0.005F127$, (b) a solution made of $TiCl_4 + 40EtOH + 0.005F127 + 10H_2O$, (c) a freshly deposited film, (d) a film aged 72 h at room tempeature, and (e) a film treated 3 h at 400 °C.

A similar behavior is suggested by EXAFS measurements (vide infra for the complete discussion of the as-deposited and treated films). The moduli of the Fourier transforms are presented in Figure 1. A first qualitative analysis shows that, when going from the precursor solution to the aged films, the intensity of the FT moduli drops. Assuming a constant coordination number of 6 for titanium, which is highly probable under such "sol−gel" conditions and confirmed by the observation of only a weak XANES preedge transition [SI], we found that this decrease indicates the presence of several subshells of neighbors, the distances and proportions of which allow a "destructive" addition of the various EXAFS modulations.[59] For the film treated 3 h at 400 °C, which corresponds to $TiO_2$−anatase (confirmed by XRD) where the six oxygen neighbors are about the same distance, the FT modulus increases again.

(48) Grosso, D.; Babonneau, F.; Soler-Illia, G. J. A. A.; Albouy, P.-A.; Amenitsch, H. *Chem. Commun.* **2002**, 748.
(49) Blanchard, J.; Ribot, F.; Sanchez, C.; Bellot, P.-V.; Trokiner, A. *J. Non-Cryst. Solids* **2000**, *265*, 83.
(50) In a water/alcohol/F127 mixture ($H_2O$:EtOH:F127 5:40:0.005 mol ratio), the water peak appears at −5.2 ppm. Addition of $H^+$ results in a shift of the $H_2O$ peak to higher $\delta$ values. For example, if 10 mol $dm^{-3}$ HCl is used, $\delta H_2O$ shifts to +4 ppm ($[H^+]/[H_2O] \approx 0.2$). Further $H^+$ addition (addition of $CH_3SO_3H$, i.e., $[H^+]/[H_2O] \approx 1.2$) results in $\delta H_2O = 18$ ppm.
(51) Teo, B. K. *EXAFS: Basic Principles and Data Analysis*; Springer-Verlag: Berlin, 1986.
(52) Rehr, J. J.; Albers, R. C. *Rev. Mod. Phys.* **2000**, *72*, 621.
(53) Michalowicz, A. *EXAFS pour le MAC*. In *Logiciels pour la Chimie*; Société Francaise de Chimie: Paris, 1991; pp 102−103.
(54) Michalowicz, A. *J. Phys. IV, France* **1997**, *7*, C2−235.
(55) Glemser, O.; Schwarmann, E. *Angew. Chem.* **1956**, *68*, 791.
(56) Yasuda, H.; Nakayama, Y.; Takei, K.; Nakamura, A.; Kai, Y.; Kanehisa, N. *J. Organomet. Chem.* **1994**, *473*, 105.
(57) Zabinsky, S. I.; Rehr, J. J.; Ankudinov, A.; Albers, R. C.; Eller, M. J. *Phys. Rev. B* **1995**, *52*, 2995.
(58) Nabivanets; Kudritskaya. *Russ. J. Inorg. Chem.* **1967**, *12*, 616.
(59) Schmutz, C.; Barboux, P.; Ribot, F.; Taulelle, F.; Verdaguer, M.; Fernandez-Lorenzo, C. *J. Non-Cryst. Solids* **1994**, *170*, 250.

**Table 1.** Results of the EXAFS Simulations

| | N | R (Å) | σ (Å) |
|---|---|---|---|
| Film Treated 3 h at 400°C: $TiO_2$−Anatase (1.8%)[a,b] | | | |
| Ti−O[c] | 6.0 | 1.96 | 0.066 |
| Ti−Ti[d] | 4.0 | 3.02 | 0.074 |
| Solution: $TiCl_4$ + 40EtOH + 0.005F127 (0.4%)[a,e] | | | |
| Ti−O[f] | 2.0 | 1.82 | 0.040 |
| Ti−O[g] | 2.0 | 2.14 | 0.050 |
| Ti−Cl[h] | 2.0 | 2.37 | 0.065 |
| Solution: $TiCl_4$ + 40EtOH + 0.005F127 + 10$H_2O$ (2.9%)[a,e] | | | |
| Ti−O[f] | 1.8 | 1.80 | 0.031 |
| Ti−O[g] | 3.5 | 2.12 | 0.130 |
| Ti−Cl[h] | 0.7 | 2.33 | 0.043 |
| Film Freshly Deposited (2.8%)[a,e] | | | |
| Ti−O[f] | 3.0 | 1.79 | 0.058 |
| Ti−O[c] | 2.0 | 1.94 | 0.036 |
| Ti−Cl[h] | 1.0 | 2.35 | 0.058 |
| Film Aged 72 h at Room Temperature (2.8%)[a,e] | | | |
| Ti−O[f] | 2.8 | 1.81 | 0.038 |
| Ti−O[c] | 2.8 | 1.95 | 0.027 |
| Ti−Cl[h] | 0.4 | 2.35 | 0.052 |

[a] Residue of the simulation: $(\sum k^4[\chi_{exp}(k) - \chi_{the}(k)]^2)/(\sum k^4[\chi_{exp}(k)]^2)$. [b] $\lambda(k)$ and $S_0^2(k)$ from $TiO_2$−anatase.[55] [c] Amplitude and phase functions from Ti−O = 1.97 Å in $TiO_2$−anatase.[55] [d] Amplitude and phase functions from Ti−Ti = 3.04 Å in $TiO_2$−anatase.[55] [e] $\lambda(k)$ and $S_0^2(k)$ from $TiCl_2(OR)_2(THF)_2$.[56] [f] Amplitude and phase functions from Ti−O = 1.79 Å in $TiCl_2(OR)_2(THF)_2$.[56] [g] Amplitude and phase functions from Ti−O = 2.20 Å in $TiCl_2(OR)_2(THF)_2$.[56] [h] Amplitude and phase functions from Ti−Cl = 2.35 Å in $TiCl_2(OR)_2(THF)_2$.[56]

For the film treated at 400 °C, the EXAFS modulations associated to the two first shells of neighbors (from 0.9 to 3.0 Å on the Fourier transforms) were analyzed with the numbers of neighbors set to the expected values (Figure 1). The found distances, reported in Table 1, agree very well with those of $TiO_2$−anatase. Attempts to simulate the third peak of the FT failed, as this contribution contains, in addition to Ti−Ti and Ti−O single scattering paths ($d$ = 3.78 and 3.87 Å, respectively), several multiple scattering paths, as was evidenced by theoretical calculations run with FEFF 7. The more important of this multiple scattering paths involves an oxygen at 1.94 Å and a titanium at 3.78 Å, which are almost aligned with the absorbing titanium (Ti−O−Ti = 155°).

For the other samples (solutions and films), only the EXAFS modulation associated to the first shell of neighbors (from ∼1 to ∼2.3 Å on the Fourier transforms) was analyzed (Figure 1). The total number of first shell neighbors was fixed at 6. The results are gathered in Table 1.

The analysis of the precursor solution, $TiCl_4$ + 40EtOH + 0.005F127, reveals three distances, each associated to two neighbors. These distances agree very well with those found in the structure of solvated titanium chloroalkoxide[47,59] (indeed, the reaction of titanium tetrachloride with ethanol is known to yield $TiCl_2(OEt)_2(HOEt)_2$).[47,60] The longer Ti−O distance (2.14 Å) corresponds to solvating molecules, ethanol or Pluronic F127.

When hydrolyzed with $H_2O/Ti$ = 10, the three same distances are still found, but their proportions change. The number of chlorides bond to titanium decreases, while the number of long Ti−O bonds increases. Moreover, this long Ti−O distance is associated to a fairly large Debye−Waller factor, indicative of disorder and an average environment due to an exchange process. Indeed, this long Ti−O distance likely involves contributions of many different groups or molecules: OTi, OH, $H_2O$, EtOH, and Pluronic F127.

The analysis of the hydrolysis−condensation behavior in solution has been supplemented by $^{17}O$ NMR spectroscopy. Addition of small water quantities ($h$ < 3, see [SI]) to a $TiCl_4$/EtOH/F127 solution (molar ratios 1:40:0.005) results in only one peak, that shifts from $\delta$ = 28 ppm ($h$ = 0.5) to 21 ppm ($h$ = 3), in a monotonic trend. Two hypotheses about this peak can be advanced: a water peak shifted by the presence of protons, or a fast exchange between Ti−OH groups (which display a chemical shift in the 200 ppm zone[61]) and water molecules. However, keeping in mind that at $h$ = 0.5, $[H^+]/[H_2O] \approx 5$, and that the water peak is indeed affected by acidity,[1] we find it easier to ascribe this effect mainly to the presence of protons in solution. For $h$ = 3, a small but fine peak begins to appear at $\delta$ = 750 ppm, a clear indication of Ti−O−Ti $\mu_2$ bridges.[37,38,49,62,63] This peak becomes more evident for $h$ > 3 [SI]. Subsequent water addition for pure $TiCl_4$ systems leads to a slight enhancement of the $\mu_2$ signal, and a shift of the water signal to lower $\delta$ ($\delta$ = 3.3 ppm for $h$ = 10, and 9.1 ppm for $h$ = 20). No other types of bridges (i.e., $\mu_3$ or $\mu_4$) are detected in pure $TiCl_4$/ethanol/water/F127 solutions. Assuming that the $\delta_{H_2O}$ shift is due to acidity, we found that these results prove that the effect of water addition (above $h$ = 3) is to raise pH (by dilution), which in turn permits a slight condensation to take place, in the form of $\mu_2$ bridges.[64]

The previous experiments demonstrate the existence of hydrolysis and a small extent of condensation in these highly acidic conditions that correspond to the initial $TiCl_4$/EtOH/$H_2O$/template solutions. Indeed, small positively charged Ti-oxo clusters[65] have been found in highly acidic aqueous media. The Ti(IV) atoms in these clusters are also connected with $\mu_2$ bridges. The only difference should be the possible coordination of chloride, in aqueous solutions, the dielectric constant of the solvent is high enough to dissociate the cationic clusters and $Cl^-$ counteranions. The presence of alcohol molecules and low water contents should favor coordination of the chloride in low quantities, even for $h$ = 10, as is evidenced by EXAFS (vide supra) and UV/vis spectroscopy (SI).

In water−alcohol solutions originating from hydrolysis of pure $TiCl_4$, condensation is not extended, and it can be proposed that small oligomeric Ti-oxo species are mainly formed. The polymerization extent should be highly dependent on pH. Similar $^{17}O$ NMR experiences have been performed using solutions containing mixtures of $TiCl_4$ and $Ti(OEt)_4$ in various ratios ($h$ = 10 in all cases; $C = [TiCl_4]/[Ti]_{total}$), to vary the

(60) Ho, H.-M.; Lee, C.-S.; Lin, C.-C.; J., M.-K.; Ho, Y.-C.; Kuo, C.-N. *J. Am. Chem. Soc.* **1996**, *118*, 2936.

(61) Blanchard, J.; Bonhomme, C.; Maquet, J.; Sanchez, C. *J. Mater. Chem.* **1998**, *8*, 985.

(62) Blanchard, J.; In, M.; Schaudel, B.; Sanchez, C. *Eur. J. Inorg. Chem.* **1998**, 1115.

(63) (a) Day, V. W.; Eberspacher, T. A.; Klemperer, W. G.; Park, C. W. *J. Am. Chem. Soc.* **1993**, *115*, 8469. (b) Chen, Y. W.; Klemperer, W. G.; Park, C. W. *Mater. Res. Soc. Symp. Proc.* **1992**, *271*, 57.

(64) It is interesting to observe that if $\delta H_2O$ is plotted against the $[H^+]/[H_2O]$-free ratio, a relatively constant $\delta H_2O$ is achieved between $h$ = 3 to 6; in the same range, the $\mu_2$ signal definitely increases. This may indicate that hydrolysis is advancing in this $h$ range and that added water is consumed to form the oxo bridges (condensation does not release protons). $[H_2O]_{free}$ is roughly estimated as the total water − (4 × [Ti]), to take into account hydrolysis. Accordingly, $[H^+]$ takes into account all protons released by the gradual hydrolysis of $TiCl_4$; please note that only hydrolysis of the chloride species brings out a proton.

(65) (a) Reichmann, M. G.; Hollander, F. J.; Bell, A. T. *Acta Crystallogr.* **1987**, *C43*, 1681. (b) Walter-Lévy, L.; Férey, G. *C. R. Acad. Sci., Ser. C* **1968**, *99*, 266. (c) Sustrino, H. Ph.D. Thesis, Institut de Matériaux de Nantes, 2001.

initial acidity.[66] Again, an intense $\mu_2$ peak is observed for $C = 1$ ($\delta = 740$ ppm), accompanied by a larger feature, that can be assigned to a superposition of different peaks. Reducing $C$ reduces acidity; consequently, $\delta_{H_2O}$ decreases, and the $\mu_2$ peak derives in a large resonance. This peak broadening has been attributed to the extension of the polymerization, which creates a larger environment distribution for the $\mu_2$ sites, and a longer correlation time (with the resulting shorter $T_2$), leading to a poor signal-to-noise ratio.[49,62] The effect of polymerization (i.e., polymer size) on the obtained NMR signal is very important. For example, $\mu_3$ and $\mu_4$ bridges are observed as broad resonances at 500−600 ppm and 320−420 ppm, respectively. However, when solutions are further diluted with ethanol, these resonances become more evident, suggesting that a rearrangement is possible, which leads to smaller Ti-oxo polymers upon dilution. Thus, the effect of proton concentration on the polymerization of these systems is considerable, and care has to be taken to determine which are the adequate initial solution conditions, to optimize film deposition. No further polymerization is detected for pure $TiCl_4$ solutions ($h = 10$) after several weeks; in contrast, for a $C = 0.125$ system, a gel is readily obtained for $h = 10$, but a solution with $h = 5$ is stable for some hours. The intermediate systems present an evolution of the polymerization state within a few days to weeks, which affects the final mesostructure, and therefore reduces the effective shelf life of the synthesis solutions. Similar results have been shown for silica sols.[31,67]

**Formation of the Hybrid Mesophases.** By the fine-tuning of the variables involved in the EISA method, $TiO_2$-based films exhibiting mesostructures from disordered wormlike (similar to that of MSU-X[11,12]) to highly organized cubic (*Im*3*m*, similar to the structure of silica SBA-16[9]) or 2D-hexagonal (*p*6*m*, similar to the structure of silica SBA-15[9]) can be reproducibly produced using a variety of PEO-based templates. Ethanol was chosen as solvent due to its surface wetting properties and the good solubility of all organic and inorganic precursors. The preferred inorganic precursor was $TiCl_4$ because the high acidity resulting from its reaction with EtOH and water quenches fast anarchic condensation. In addition, the HCl produced in situ is volatile and can be eliminated during the evaporation process, allowing extended inorganic polymerization. Working with this system, six (main) variables should be precisely controlled to allow the production of highly organized, good optical quality coatings, and to control the final mesophase: (1) the choice of the template, (2) the $s$ = template/metal ratio, (3) the quantity of water inside the solution, (4) the quantity of water in the atmosphere (i.e., the relative humidity), (5) the solution acidity (which can be controlled by using $TiCl_4/Ti(OEt)_4$ mixtures), and (6) the temperature during deposition and aging.[68] To study the role of these parameters, a combination of time-resolved 2D-SAXS and interferometry was applied to evaluate the mesophase formation related to the evaporation process. These techniques were crossed with mass spectrometry (MS), energy-dispersive X-ray spectroscopy (EDX), ellipsometry, EXAFS, and FT-IR, leading to a better understanding of the formation path.

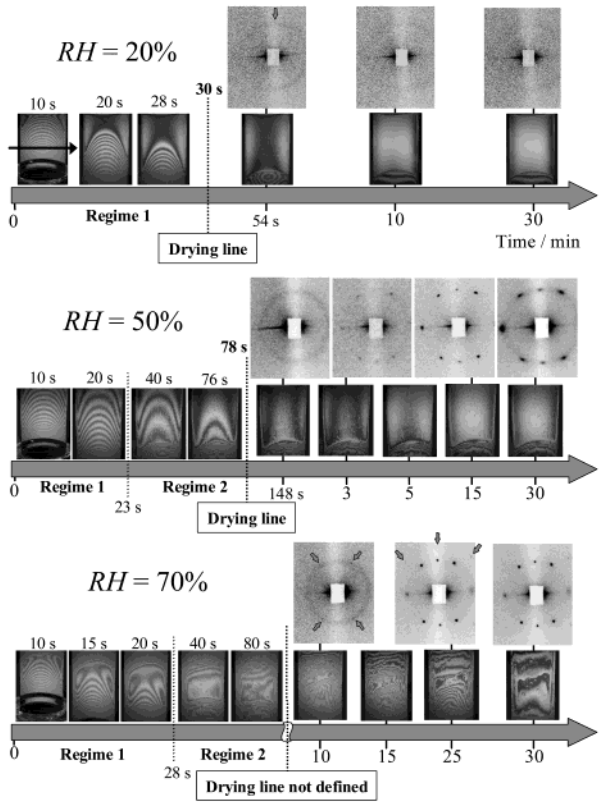


***Figure 2.*** In-situ 2D-SAXS and interferometry results taken for B58-templated $TiO_2$-based films during dip-coating at different RH. Films were prepared at 23−24 °C, from solutions containing $TiCl_4$, $s = 0.05$, and $h = 10$.

**Formation Path.** Using $TiCl_4$ as the inorganic source, we obtained very acidic solutions, in which water can be added resulting in hydrolyzed (thus, hydrophilic) inorganic moieties, while inorganic polymerization is quenched.[43] Besides the effect of water added in solution, in EISA-derived methods, and particularly for the formation of films, the exchange of water between the coating and its environment is enhanced by the high surface/bulk ratio associated to films. As a result, the relative humidity (RH) in which EISA is performed is crucial. Indeed, this phenomenon is clearly illustrated by the in situ SAXS and interferometry results, which are shown in Figure 2.

Five regions could be identified during the evaporation process (Figure 2), which are schematically represented in Figure 3a. The data obtained by MS, EDX, and Karl Fisher experiments can give a good idea of how the volatile species depart from the film (see Figure 3b and c). The fast decrease in the film thickness observed in region 1 can be assigned to the evaporation of ethanol-rich vapors from the $EtOH/H_2O/HCl$ mixture. In region 2, a second and slower evaporation process was observed, which can be attributed to the departure of $H_2O/HCl$-rich vapors from the same mixture, and no mesophases were detected.

This region is detected only for RH ≥ 45%, suggesting that it is associated to the diffusion of water from the atmosphere within the coating. After the drying line (region 3), when the film thickness practically does not vary anymore, a broad

(66) Tian, B.; Yang, H.; Liu, X.; Xie, S.; Yu, C.; Fan, J.; Tu, B.; Zhao, D. *Chem. Commun.* **2002**, 1824.
(67) Birnbaum, J. C.; Li, X.; Yonker, C. R.; Fryxell, G. E.; Baskaran, S. *Chem. Commun.* **2002**, 2270.
(68) Please note that temperature also affects the water partial pressure at equilibrium: a higher water quantity (i.e., partial pressure) will be present at a given RH at a higher temperature. This will affect direct comparison of RH conditions at different temperatures; in this paper, we will describe RH effects for experiments made at the same temperature.

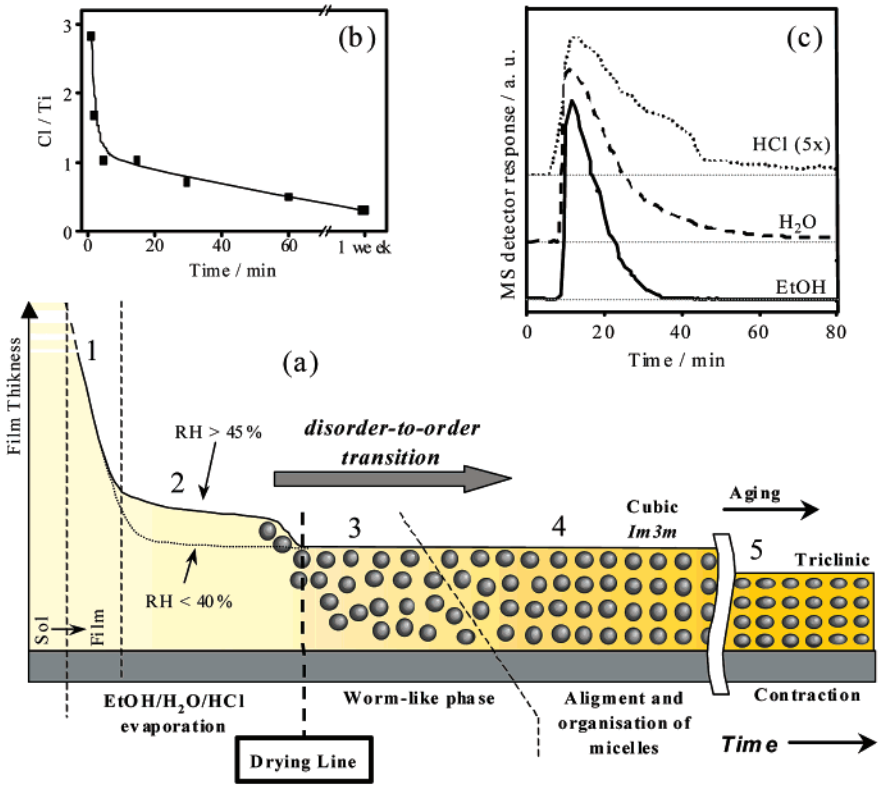


***Figure 3.*** (a) Scheme representing the stages of film formation during dip-coating. (b) EDX analysis of the Cl/Ti ratio as a function of time for B58-templated $TiO_2$ films prepared following the conditions described in Figure 2, and at RH = 50%. (c) Evolution of the volatile species as determined by mass spectrometry for the same conditions (see Experimental Section for more details).

diffusion ring can be observed in the SAXS pattern, which is characteristic of randomly oriented mesostructure domains.[30]

At this point, micelles are already formed, displaying a defined size, an average interdistance, and random orientation. From the SAXS data, it is impossible to differentiate between a wormlike phase formed by disordered channels or a disordered stacking of spherical micelles. Even though at this point only residual amounts of solvent (mainly water, as revealed by Karl Fisher experiments) are still present in the film, the structure displays high mobility (depending on the quantity of water inside the films and thus on RH), and along region 4 the micellar aggregates organize and align (along the film/substrate and film/air interfaces), resulting in a transition from wormlike to cubic (*Im*3*m*, see below), as is evidenced by the defined diffraction spots in the SAXS patterns. In region 5, residual amounts of water and HCl depart from the film, allowing further condensation, which in turn results in the stabilization and contraction of the structure.

This formation path, characterized by a disorder-to-order transition,[69] can be generalized to all systems studied here and also to the formation of poly(ethylene oxide)-based ABC-templated mesophases of other transition metal oxides (such as $ZrO_2$,[40,70] $Al_2O_3$,[41] $VO_x$,[42] and mixed oxides[70])[71] and silica,[33] besides the different chemical behavior of these systems. However, the continuity of this process until the formation of an organized mesostructured hybrid is highly dependent on the applied conditions, as one can see in Figure 2, exemplified by the role of RH. The role of each of the variables will be discussed in detail below.

**A Detailed View of the Mesostructure As Revealed by SAXS, XRD, and TEM.** Figure 4a shows a typical SAXS pattern for a cubic mesostructured hybrid film, showing diffraction spots with related distances ratio and angles in agreement with a body-centered cubic mesophase (*Im*3*m* space group) with [110] planes parallel to the substrate (see Figure 4c). This phase was found with the same orientation for F127-templated silica films.[34] This orientation seems to be the same as that reported for Pluronic P123 ($EO_{20}PO_{70}EO_{20}$)-templated *Im*3*m* mesoporous silica and titania films;[44] however, in such a work, the indexation is misleading (the authors indexed spots distributed along an ellipse as different orders, which shows they are unaware of the anisotropic contraction that takes place in these systems, see below). Another orientation for this same structure, with the (100) planes parallel to the substrate, was also reported for F127-templated silica films.[32]

SAXS patterns collected in incidence normal to the substrate showed diffraction rings, indicating that the **c** vector has no particular orientation along the deposition direction.[34] It means that the film/substrate and the film/air interfaces are the driving force governing the alignment of the micelles (in particular, the alignment of the most densely packed planes in the cubic lattice). In the formation of such films, the shearing forces induced by the drainage of the solution toward the deposition direction have no influence on the structural alignment. This fact is in agreement with the in situ SAXS experiments, which showed that organization starts after the (almost) complete

(69) Yao, N.; Ku, A. Y.; Nakagawa, N.; Lee, T.; Saville, D. A.; Aksay, I. A. *Chem. Mater.* **2000**, *12*, 1536.
(70) Crepaldi, E. L.; Soler-Illia, G. J. de A. A.; Grosso, D.; Durand, D.; Sanchez, C. *Angew. Chem., Int. Ed.* **2003**, *42*, 347.
(71) Crepaldi, E. L.; Soler-Illia, G. J. A. A.; Grosso, D.; Albouy, P.-A. *Stud. Surf. Sci. Catal.* **2002**, *141*, 235.

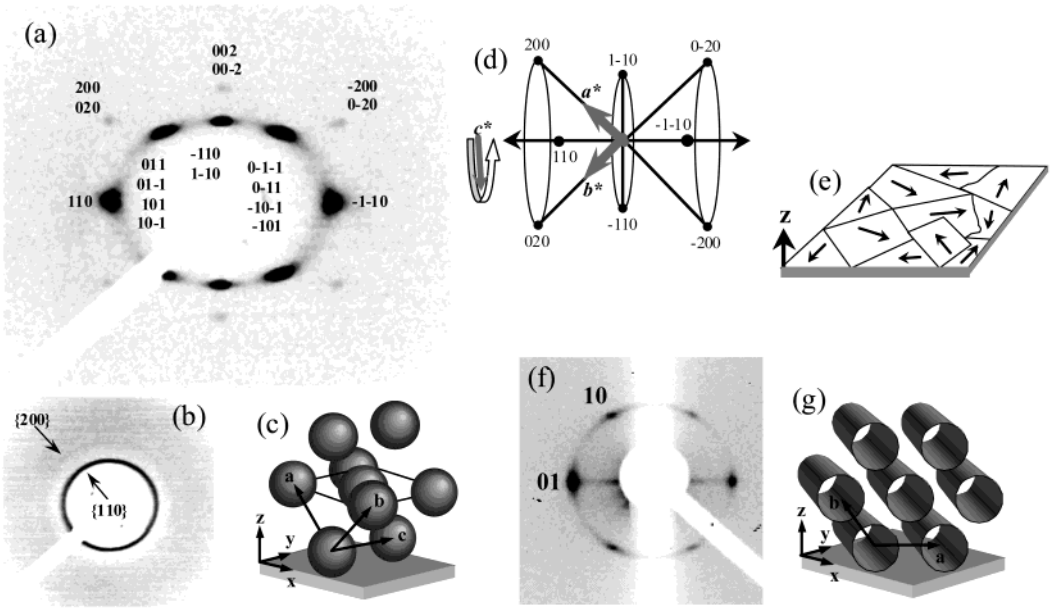


***Figure 4.*** Indexed SAXS patterns, collected at (a) 4° and (b) 90° incidence angles, of a cubic *Im*3*m* F127-templated $TiO_2$-based film prepared from a solution containing $TiCl_4$ as the inorganic source, $h = 10$, and $s = 0.005$. The film was deposited and aged for 1 week at RH = 50%. The nonindexed spots correspond to the other half of the circles shown in (d). (c) Schematic representation of cubic domains. (d) Scheme of the reciprocal space, showing the {200} and some of the {110} planes as an example. As a result of the rotation of the *c* axis, some of these planes are polyoriented; in the reciprocal space, this is translated as concentric circles. The result of the intersection of the Ewald sphere and these circles in grazing incidence is the pattern observed in (a). (e) Schematic representation absence of in-plane orientation (represented by the **c** vector, with **c**⊥**z**, **z** is normal to the substrate). (f) Indexed SAXS pattern, collected at a 4° incidence angle, of a 2D-hexagonal *p*6*m* B56-templated $TiO_2$-based film prepared from a solution containing $TiCl_4$ as the inorganic source, $h = 10$, and $s = 0.20$. The film was deposited at RH = 50%. (g) Scheme representing the alignment of the 2D-hexagonal domains to the substrate.

***Table 2.*** Structural Characteristics of As-Prepared $TiO_2$ Films Obtained with Various Templates[a]

| template | $s$[b] | $s_C$[c] | $a_C$/Å | $s_H$[c] | $a_H$/Å | $s_L$[c] | $a_L$/Å |
|---|---|---|---|---|---|---|---|
| Brij 56 | 0.05−0.40 | 0.10−0.15 | 89−98 | 0.20−0.3 | 90−104 | >0.30 | 100−104 |
| Brij 58 | 0.03−0.20 | 0.04−0.07 | 82−96 | 0.10−0.15 | 75−81 | | |
| Pluronic P123 | 0.003−0.040 | | | 0.05−0.09 | 138−151 | ≥0.10 | 159−163 |
| Pluronic F127 | 0.001−0.020 | 0.003−0.006 | 179−195 | 0.008−0.010 | 167−189 | | |

[a] Films were prepared from solutions containing $TiCl_4$ as the inorganic source, $h = 10$, and RH = 50%. C = cubic *Im*3*m*, H = 2D-hexagonal *p*6*m*, L = lamellar. [b] Tested range. [c] "Ideal" range.

departure of the solvent, where no more drainage movement is expected.

Figure 4f shows a typical 2D-SAXS pattern of a 2D-hexagonal mesostructured hybrid film. In this pattern, six spots with angles in agreement with a *p*6*m* mesophase, with the (01) planes aligned parallel to the substrate, can be observed. The complete indexation of such a phase in the same orientation can be found in many previously reported works for a variety of metal oxide/template systems.[30−33,39,40,44] As for the cubic mesophase, the most densely packed planes in the hexagonal lattice align parallel to the substrate, stressing again the role of the film/substrate and film/air interfaces as the alignment driving force. SAXS patterns collected at 90° showed a diffraction ring, indicating that the *c* axis has no preferential orientation along the deposition direction,[30] as was observed for the cubic *Im*3*m* phase.

By analyzing the SAXS patterns displayed in Figure 4, one can see that the spots of the same order are not distributed along a circle but along an ellipse, with the in-plane spots, resulting from the planes parallel to the substrate, presenting a slightly smaller distance than the out-of-plane spots (the distortion is higher for the F127-templated film due to aging). This distortion of the structure is caused by an anisotropic contraction, which in turn results from the adhesion of the film to the substrate (see below). Therefore, nondistorted cubic or 2D-hexagonal mesophases are only observed for freshly formed films, and the distortion leads, respectively, to a triclinic (*P*1 space group) or a 2D-centered rectangular (*C*2*m* space group) mesostructure.

Table 2 summarizes the typical structural parameters obtained with a variety of templates. The presented ranges reflect the effect of *s* on the final structure. Larger *d*-spacings are obtained at higher humidity (see, for instance, the SAXS patterns obtained for 50% and 70% RH in Figure 2). The swelling effect of water molecules, induced by the RH, can be retained if the film is aged in the same atmosphere for at least 1 h.

TEM images of stabilized (at 130 °C) cubic films are presented in Figure 5. Periodicities found by TEM and SAXS agree within 10% (179 and 186 Å by TEM and SAXS, respectively). Such small differences might arise from tilting and focusing effects associated to TEM analyzing, or sample shrinking caused by the heat induced by the electron beam. In the case of hexagonal phases, data agree with previously reported results.[39]

**The Effect of the Experimental Parameters. The Critical Role of Water.** Using the optimal conditions (vide supra), we

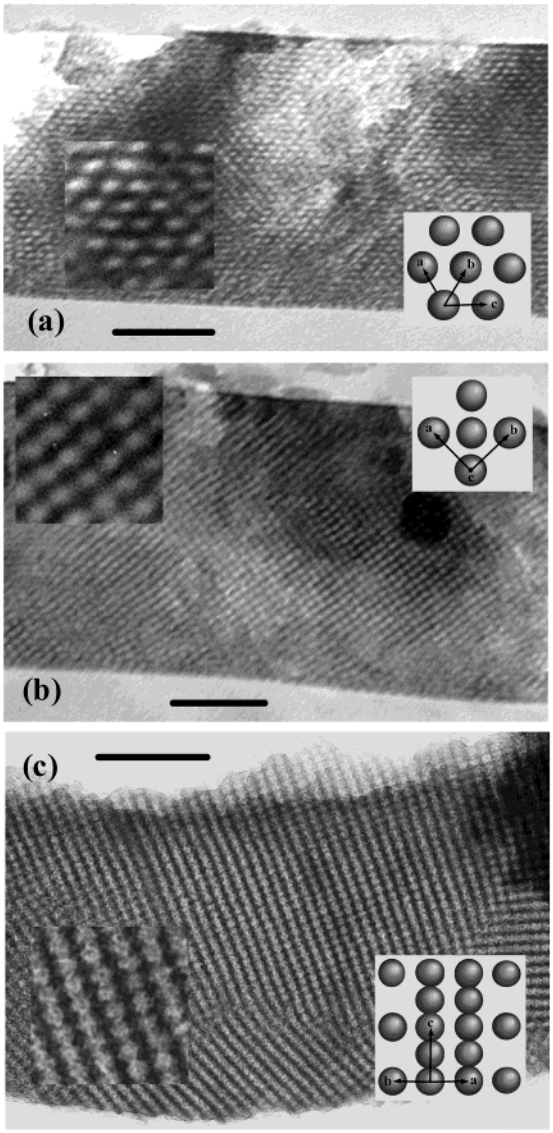


***Figure 5.*** TEM images of a 130 °C stabilized F127-templated $TiO_2$-based film prepared as was described in Figure 4. The images are cross sections perpendicular to the (a) [111], (b) [100], and (c) [110] directions. The insets in both parts show a magnification of a selected region and a scheme of the projection. Scale bars are (a) 50 nm, (b, c) 100 nm.

eliminated most of the HCl during the first minutes after dip-coating (see Figure 3b and c). The formation of extended titanium-oxo polymers is dependent on concentration and pH.[72] During evaporation, condensed $TiO_{2-x/2}(OH, Cl)_x$ species are formed,[43,73] as was checked here by $^{17}O$ NMR. In acidic medium, discrete closo objects (hydrophilic nanoparticles or clusters of ca. 2 nm gyration radius) have been characterized by SAXS[74] and are likely formed during the process described here, as was previously discussed for the formation of $TiO_2$/CTAB mesostructured xerogels.[43] However, FT-IR spectra of freshly deposited (from 15 min to 1 h) films, in equilibrium with a RH = 50% atmosphere, show the presence of a very strong and broad band around 3400 $cm^{-1}$ ($\nu$O−H), and a very weak band around 450 $cm^{-1}$ (Ti−O−Ti), indicating a low degree of condensation of the inorganic framework. Even though most of the HCl is eliminated during the evaporation process, the quantity that remains in the film (at RH = 50%, 1Cl/Ti after 3 min and 0.7 after 1 h) after the drying line is confined to a very small volume. This high local concentration of HCl hinders extended inorganic polymerization from several minutes to days. Meanwhile, the formation of a liquid crystal phase of the template is possible. The SAXS data displayed in Figure 2 clearly show that, in such conditions, template nanosegregation is mainly governed by the humidity in the atmosphere, which encourages water to quickly evaporate (low RH) or to stay inside the coating (high RH).

To understand the role of water in these systems, a "map of organization" was constructed by varying $h$ in the 0−20 range and RH in the 10−80% range, using the intensity of XRD peaks[75] (in $\theta-2\theta$ mode) as a parameter for order (taking into account that more intense peaks are also narrower), and checking some points by 2D-SAXS. Selected results are shown in Figure 6.

Results displayed in Figure 6a show that the sol water content does influence the organization, with a maximum of order in the $h$ = 7−15 range. It is confirmed by the SAXS patterns, following parts b, c, d, and e in Figure 6. On the other hand, this effect is minor when compared to the role played by atmospheric moisture. Indeed, fixing an "ideal" value for $h$, at 10, the SAXS patterns following parts f, g, e, and h in Figure 6 clearly show a very high improvement in organization. Totally nonorganized coatings are obtained for RH ≤ 15%, a disordered mesostructure at RH = 20%, and cubic mesostructures with increasing organization as RH further increases.

These results show that the quenching of condensation given by the acidic medium is necessary but not sufficient to permit the disorder-to-order transition. In addition, a substantial quantity of water must be present to guarantee the necessary fluidity that will permit the organization of the template in a liquid crystal phase. Karl Fisher and ellipsometry experiments confirmed that the amount of water in the coating is directly associated to the RH (see Table 3) (for RH = 70%, it corresponds to about 50% of the film mass after the drying line).[76] Recently reported results for CTAB-templated silica[76] and ABC-templated zirconia[70] systems point in the same direction. Even for the silica/CTAB system, in which template nanosegregation is much faster, a minimum amount of water in the deposited gel is necessary to allow template nanosegregation.[76]

The role of water in the formation of highly organized ABC templated $TiO_2$-based mesostructured films is multiple. Water, incorporated in solution and provided by air moisture, hydrolyzes the inorganic species, making them hydrophilic and enhancing their interactions with the hydrophilic portion of the ABC.[37,38] The enrichment of the system in water also favors condensation, which can be maintained under control by working in acidic medium. After the drying line, a relatively high amount of water remains within the film if the atmosphere inside the dip-coater chamber is humid (RH > 40%). During

(72) Baes, C. F.; Mesmer, R. E. *The Hydrolysis of Cations*; John Wiley & Sons: New York, 1976.
(73) Jolivet, J.-P. *Metal Oxide Chemistry and Synthesis: from Solution to Solid State*; John Wiley & Sons: Chichester, 2000.
(74) Kalalla, M.; Sanchez, C.; Cabane, B. *Phys. Rev. E* **1993**, *48*, 3692.
(75) For B58-templated $TiO_2$ films, deposited from solutions as described in Figure 8 and at room temperature, the acquired structure can vary from disordered to highly ordered cubic (*Im*3*m*), depending on $h$ and RH. For these films, XRD patterns in the $\theta-2\theta$ mode display a single peak, which corresponds to the in-plane spots (110) in the 2D-SAXS patterns.
(76) Cagnol, F.; Grosso, D.; Soler-Illia, G. J. A. A.; Crepaldi, E. L.; Babonneau, F.; Amenitsch, H.; Sanchez, C. *J. Mater. Chem.* **2003**, *13*, 61.

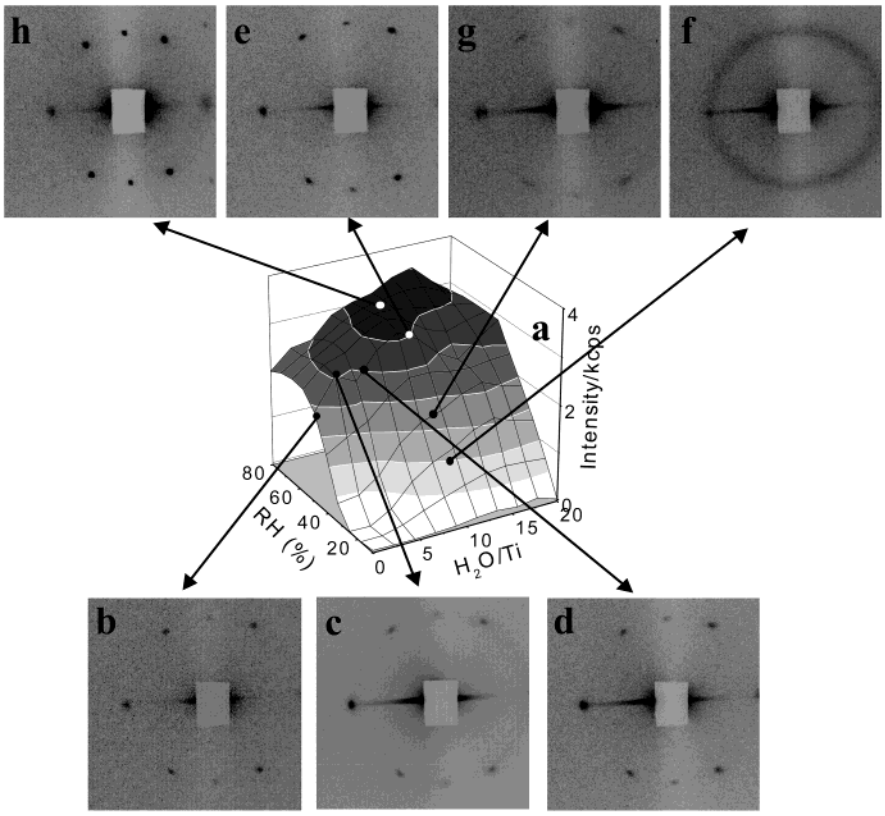


***Figure 6.*** A "map of organization" as a function of $h$ and RH (a), using the intensity of the XRD peak (in $\theta-2\theta$ mode) as a parameter for order, for B58-templated $TiO_2$-based films prepared at 23−24 °C and using $TiCl_4$ as the inorganic source and $s = 0.05$. From (b) to (h) are displayed 2D-SAXS patterns, collected in transmission mode (incidence of 4° to the substrate) 15 min after the deposition start, for films prepared in selected conditions, as indicated.

***Table 3.*** Water Content (Karl Fisher) and Film Thickness (Ellipsometry) for Fresh F127-Templated Films as a Function of RH

| RH (%) | water content (%)[a] | film thickness/nm[b] |
|---|---|---|
| low (2−20) | 15 ± 5 | 150 |
| medium (40−60) | 30 ± 15 | 220 |
| high (70−80) | 50 ± 10 | 320 |

[a] Karl Fisher titration. [b] Measured by ellipsometry; see Experimental Section for the complete procedure.

this dynamic equilibrium state, the fluidity of the deposited gel layer is high enough to permit template self-assembly and the formation of organized mesophases. Also during this stage (i.e., a few minutes to approximately 1 h after deposition), the continuous exchange of water between the film and the atmosphere favors the progressive departure of HCl (as was observed by EDX, see Figure 3b), allowing condensation of the inorganic framework around the micellar aggregates.[77]

In addition, the quantity of water inside the hybrid coating can control the structure of the final mesophase. For ABC-templated trivalent metal (Y(III) or Ce(III)) containing zirconia-based mesostructured films,[70] the cubic to 2D-hexagonal (or reverse) phase transition can be controlled by the RH in the atmosphere at a fixed $s$. The same effect is observed for silica/CTAB systems.[76] The phase transition occurs as an effect of the elimination or addition of water (1) inside the inorganic network, (2) between the PEO polar chains, and (3) at the hybrid interface. As a result, the template volume fraction [$\Phi_T$, defined as the ratio $V_{template}/(V_{template} + V_{inorganic})$][44] and the amount of interface change, favoring a higher (cubic, through incorporation of water) or lower (2D-hexagonal, through elimination of water) curvature of the micelles. $TiO_2$-based systems are more restrictive. The inorganic framework of the $TiO_2$-based films, in many situations, reaches a condensation degree that is enough to hinder a phase transition even a few minutes after deposition. For instance, the cubic to 2D-hexagonal phase transition in freshly deposited films cannot be induced by a fast decrease in humidity (from 50% to 10%), contrary to what was observed for other systems.[70] Notably, Ti(IV) cations are known to condense slower than Zr(IV) cations in similar concentration and pH conditions.[72,73,78] Nevertheless, oxolation predominates during Ti(IV) condensation, leading to stable Ti-oxo-bridges. This can explain the "mesophase stability" for freshly formed $TiO_2$-based coatings. For $ZrO_2$-based systems, the very fast condensation consists mainly in olation reactions,[78] and the freshly formed Zr-hydroxo-polymers can be "redissolved".[40,70,77] This reversibility allows the humidity-induced mesophase transition, while further oxolation, which is thermodynamically favored, stabilizes the mesophase as time goes on.[70]

**The Role of Acidity.** Reducing the acidity of the solution, by using $TiCl_4/Ti(OEt)_4$ mixtures, has, in general, a detrimental effect on the organization [SI]. Practically no organization is attained for a Cl/Ti ratio in solution lower than 1 ($TiCl_4/Ti_{total} = 0.25$). For higher acidity, organization is obtained, and a local maximum in order exists for $TiCl_4/Ti_{total} = 0.5$ and $h = 0$.

(77) Crepaldi, E. L.; Soler-Illia, G. J. de A. A.; Grosso, D.; Sanchez, C. *New J. Chem.* **2003**, *27*, 9.

(78) Larsen, E. M. In *Advances in Inorganic Chemistry and Radiochemistry*; Emeléus, H. J., Sharpe, A. G., Eds.; Academic Press: New York, 1970; Vol. 13, p 1.

Indeed, when $TiCl_4/Ti_{total} \leq 0.5$, the addition of water in solution leads to lower organization,[79] and the solutions are stable for only a few days or even hours, both effects as a consequence of fast inorganic polymerization (vide supra). The quality of organization for mesophases obtained for $0.25 < C < 1$ depends on solution aging, and thus on the condensation kinetics of Ti(IV) species.

Therefore, the indiscriminate condensation that takes place in low acidic medium can hinder the disorder-to-order transition before the formation of organized mesophases, "freezing" intermediate disordered states.[70,79] Better results are obtained when high molecular weight Pluronic ABCs are used instead of Brij. These templates probably can better accommodate the larger $TiO_2$ nanobuilding blocks, which are likely to be formed in low acidic medium (see the $^{17}O$ NMR section).[49,62,73] Indeed, coatings presenting relatively high order can be obtained when F127 is used as template and $TiCl_4/Ti_{total} \geq 0.25$, with $h = 0$ and high humid atmosphere (RH > 45%). Nevertheless, the highest degree of organization was reached for very acidic medium ($TiCl_4/Ti_{total} = 1$) for all of the studied templates.

**Effects of the Template and Template/Ti Ratio (*s*).** The parameter *s* must be fixed above a critical value (see Table 2) to allow organization, as was previously observed by Chmelka and co-workers.[35] At lower *s*, nonorganized or ill-defined wormlike structures are obtained. The choice of the template and its ratio to the inorganic species is recognized to be main parameters in controlling the final mesostructure.[44,80] If the experimental conditions are fixed so that the disorder-to-order transition is not stopped, the final mesophase can be precisely controlled by these parameters. ABCs presenting high hydrophilic/hydrophobic ratios (such as B58 and F127) favor cubic *Im*3*m* mesophases. In Table 2 are listed the ideal ranges of *s* for obtaining highly ordered cubic mesophases. Inside these ranges, a phase transition from cubic to 2D-hexagonal can take place only if the temperature is quickly increased.[39] At higher *s*, B58- and F127-templated films present 2D-hexagonal structure. For B56, the cubic mesophases are, in general, less ordered than those obtained with B58 or F127. For P123, a cubic mesophase could not be stabilized, even at very low *s*, which differs from the results obtained by Alberius et al.[44] These authors used a low temperature of aging, which seems to be the key for such a task. Indeed, B56 and P123 favor 2D-hexagonal mesostructures and lamellar phases at high *s*.

The formation of 2D-hexagonal mesophases takes place by the same pathway described above for the formation of the cubic mesophases, except that, in a certain stage, the spherical micelles in the cubic phase coalesce along the [1-11] direction (following the orientation represented in Figure 4c), giving rise to modulated cylindrical micelles and finally strait cylindrical micelles,[34,70] as was reported for ABC/water systems.[81] This epitaxial relation (Figure 7), characteristic of all templates used in this work, leads to a fast transition, which takes place in a few seconds, and the detection of the intermediate states is very difficult. Even with SAXS patterns recorded every 1 s, diffraction spots characteristic of both mesophases were detected. This suggests that this transition is not homogeneously distributed

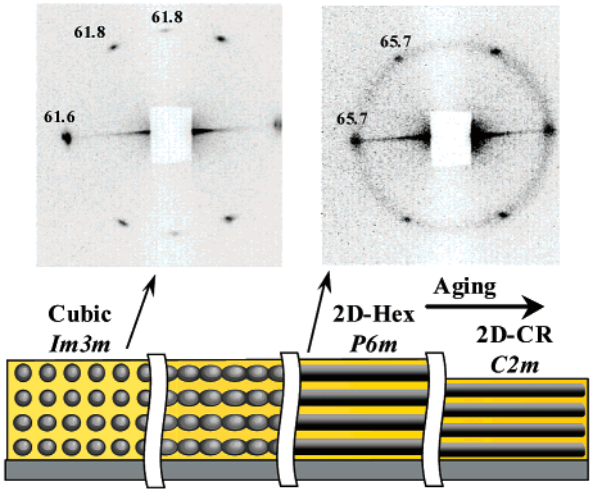


***Figure 7.*** (Bottom) Scheme representing the cubic to 2D-hexagonal mesophase transition. This scheme is complementary to that shown in Figure 4. (Top) 2D-SAXS patterns acquired during the formation of a B58-templated $TiO_2$-based mesostructured film (left) 8 min and (right) 10 min after the deposition. $TiCl_4$ was used as the inorganic source, $s = 0.10$, and $h = 10$. The deposition was carried out at 24 °C and RH = 50%. Distances are given in angstroms.

throughout the coating; in no case were patterns observed that could be related to the modulated cylindrical micelles claimed to be the intermediate state.[81] This epitaxial relation is responsible for the presence of the same type of orientation, with the most densely packed planes aligned along the substrate, for both mesophases. As a result, the SAXS patterns of both mesophases are similar. When only the first-order spots could be detected, the main difference is the presence of spots at 90° to those in-plane in the 2D-SAXS patterns of the cubic mesophase. Furthermore, the *d*-spacings (but not necessarily the interpore distance) are larger in the case of the 2D-hexagonal mesophase for a given *s* (see Figure 7).

The cubic to 2D-hexagonal phase transition is favored for B56 and P123 in a range of *s*, but for B58 and F127, high ratios are necessary to induce such a transformation. Indeed, for B58 and F127, with *s* fixed at or below 0.08 and 0.007, respectively, this transition can be avoided if the humidity is raised to more than 60%. This result shows that the final mesophase is always controlled by $\Phi_T$, as was previously reported by Stucky and co-workers.[44] Nevertheless, these authors claimed that, by fixing *s* in the initial solutions, all mesophases present in the phase diagram of P123/water[82] can be selectively formed. In view of the results presented here and elsewhere,[34,70,76] this approach is rather simplistic once one considers that the volume of the inorganic nanophase is invariable; our results clearly show that $\Phi_T$ can be controlled by varying the volume of the inorganic phase by changing the humidity of the atmosphere. Working at high humidity, water is encouraged to stay inside the coating, favoring the formation of micelles of high curvature (cubic mesophase); during this dynamic equilibrium state, condensation progressively takes place, stabilizing the inorganic framework

(79) Soler-Illia, G. J. A. A.; Grosso, D.; Crepaldi, E. L.; Cagnol, F.; Sanchez, C. *Mater. Res. Soc. Symp. Proc.* **2002**, *726*, 243.
(80) Huo, Q.; Margolese, D. I.; Stucky, G. D. *Chem. Mater.* **1996**, *8*, 1147.
(81) Sakya, P.; Seddon, J. M. M.; Templer, R. H.; Mirkin, R. J.; Tiddy, G. J. T. *Langmuir* **1997**, *13*, 3706.
(82) Holmqvist, P.; Alexandridis, P.; Lindman, B. *J. Phys. Chem. B* **1998**, *102*, 1149. For phase diagrams of block copolymers in different solvents, see also: (a) Wanka, G.; Hoffmann, H.; Ulbricht, W. *Macromolecules* **1994**, *27*, 4145. (b) Alexandridis, P.; Zhou, D.; Khan, A. *Langmuir* **1996**, *12*, 2690. (c) Alexandridis, P.; Olsson, U.; Lindmann, B. *Langmuir* **1998**, *14*, 2627. (d) Ivanova, R.; Alexandridis, P.; Lindmann, B. *Colloids Surf., A* **2001**, *183−185*, 41. For a recent review: Ivanova, R.; Alexandridis, P.; Lindmann, B. *Adv. Colloid Interface Sci.* **2001**, *89−90*, 351.

around the spherical micelles and avoiding phase transition when RH is lowered or when the temperature is increased (see below).

The external conditions, especially the RH, are likely to be "the lost link" to the reproducible controlled formation of mesostructured thin films.[34,70,76] A good example of that is the different results obtained by Zhao et al.[32] (cubic mesophase) and Grosso et al.[33] (2D-hexagonal mesophase) when working with F127/silica systems and applying the same conditions, including the inorganic source, *s*, *h*, ethanol/Si ratio, substrate, and temperature during deposition. Therefore, the approach based on fixing *s* to control the final mesophase should be complemented by a series of other variables (many times neglected such as RH) to be able to give rise to reproducible results, independent of operational, geographical, or seasonal features.[83]

**Effect of the Temperature during Dip-Coating.** As discussed above, the disorder-to-order transition can take place if the fluidity of the coating is kept high enough to permit template self-assembly. For that, inorganic polymerization must be quenched and an important amount of water must remain inside the coating for at least 10−15 min after deposition. Therefore, increasing the temperature, which induces faster evaporation (associated to a better optical homogeneity) and increases condensation rate, is detrimental to the formation of organized mesostructured films; this detrimental effect of temperature on organization has also been observed in thick films.[43] The best results for combining good optical quality and organization in the final coatings were obtained from 20 to 30 °C. Temperatures higher than 40 °C hinder meso-organization.

A mesophase transition (cubic to 2D-hexagonal) can be promoted for B58 and F127 with *s* inside the ideal range for the formation of cubic mesophases (0.05 and 0.005, respectively) by a fast increase in temperature (for films prepared at RH = 50−70%) a few minutes (5−20) after the deposition start, as was previously reported.[39] For that, the freshly deposited films were removed from the dip-coater chamber and placed inside an oven at 60 °C. The phase transition, which takes place around 40 °C, is very fast and occurs before departure of the solvent and condensation of Ti-oxo species, induced by a change in curvature of the micellar aggregates as a result of a change in the conformation of the PEO chains.[81,82,84]

**Liquid Crystal Behavior of the Hybrid Films: Possibilities of Postprocessing.** The low degree of condensation attained during the first minutes that follow the deposition process confers high flexibility to the mesophase. As discussed above, the inorganic framework is composed of low condensed species and an amount of water that varies along with the humidity in the atmosphere in contact with the film, with interpenetrated template PEO chains. As such, the mesophases are similar to those obtained by mixing PEO-based ABCs with hydrated bivalent metal salts.[85] Those are "metallotropic" liquid crystals. The freshly prepared mesostructured films obtained here can be considered as "titanotropic" phases. Indeed, when 2D-hexagonal mesophases are obtained, the films are birefringent to polarized light.

An example of the mesostructural mobility is given in Figure 8. With a variation in the RH after the formation of an organized mesophase, the coating absorbs water and swells as the humidity is raised, and loses water and contracts as the humidity drops. The degree of mobility is progressively lost with time, as a result of inorganic polymerization.

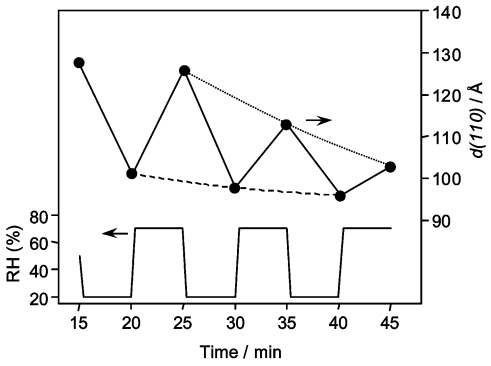


***Figure 8.*** Variation of *d*-spacing, determined by SAXS, for a F127-templated $TiO_2$-based mesostructured film deposited at RH = 50% as a function of the applied RH and time ($TiCl_4$ as the inorganic source, $h$ = 10, and $s$ = 0.005). RH = 50% was maintained for 15 min after deposition and then quickly varied between 20% and 70%. Once the desired humidity was reached, it was kept for 5 min for equilibration, and a SAXS pattern was recorded. The dotted line (points acquired at RH = 70%) and the dashed line (data acquired at RH = 20%) are a guide for the eye.

We observed that one can take advantage of this mobility to enhance the optical quality of the coatings. The better quality of the coatings deposited at low RH can be seem in Figure 2. Films deposited at high RH are transparent, but present a nonhomogeneous thickness [SI], as a consequence of the slow drying related to the absorption of water during the formation of the layer. On the other hand, films deposited in RH < 45% are of excellent optical quality [SI], but present a wormlike structure. An alternative method for obtaining high optical quality (homogeneity) and excellent organization consists of making a deposition at low RH and a postprocessing at high RH [SI]. This high RH posttreatment is much more efficient if applied as soon as possible, to avoid the condensation of the inorganic framework, which can "freeze" the intermediate disordered structure.[40,70]

**Aging and Mesostructural Stabilization.** Because the as-prepared film is weakly condensed, it presents a relatively fragile mesostructure. As a consequence, the treatment method chosen to eliminate the volatile species, to increase the condensation of the inorganic moieties up to crystallization and to eliminate the template, is of paramount importance because it determines the integrity of the organization, the degree of contraction, and the thermal stability of the final mesoporous coating.

Therefore, a set of aging treatments under controlled relative humidity followed by progressive thermal treatments (from 60 to 130 °C) was carried out, which is crucial for the formation of highly organized, high surface area semicrystalline coatings during heating treatments at temperatures in excess of 350 °C (see below). The importance of these aging treatments was discussed in a previous communication.[77]

**Thermal Treatment. Stability of the Mesostructure.** To prestiffen the network in the desired mesostructure, it is necessary to age the film for at least 24 h at the required humidity. After that, it is stable enough to be calcined. Heating induces further condensation, which stabilizes the coating and causes structural contraction. As a result of the adhesion of the film to the substrate, contraction occurs in the direction normal

(83) Alonso, B.; Balkenende, A. R.; Albouy, P.-A.; Durand, D.; Babonneau, F. *New J. Chem.* **2002**, *26*, 1270.
(84) Guo, C.; Liu, H. Z.; Chen, J. Y. *Colloid Polym. Sci.* **1999**, *277*, 376.
(85) Çelik, Ö.; Dag, Ö. *Angew. Chem., Int. Ed.* **2001**, *40*, 3800.

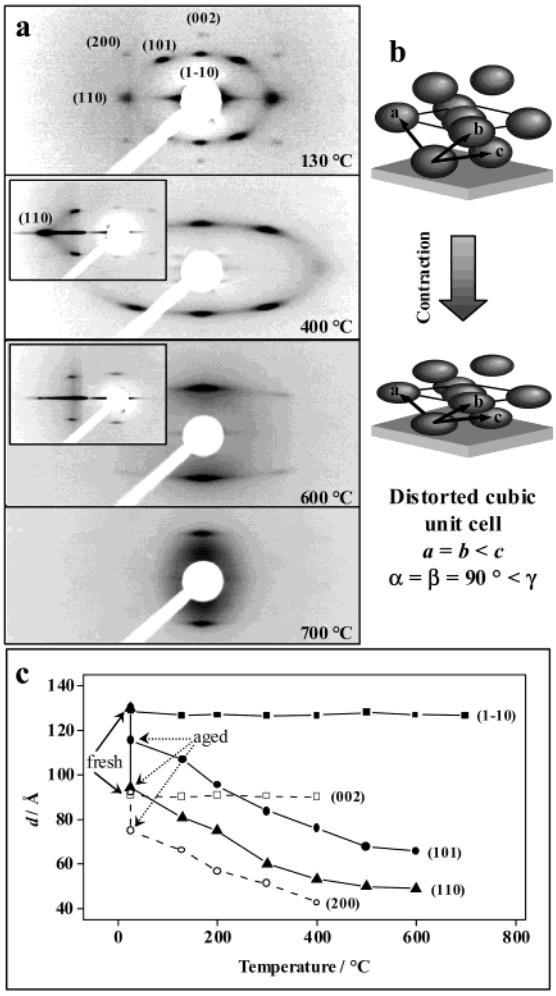


***Figure 9.*** Typical results obtained during calcination of films exhibiting a cubic mesostructure. The example here is a F127-templated film. (a) 2D-SAXS patterns (4° incidence angle) of the film treated at different temperatures. The insets in (a) are patterns taken at grazing incidence. (b) Schematic representation of the distorted cubic structure observed after the anisotropic contraction. (c) Variation of *d*-spacing as a function of temperature, clearly showing the uniaxial contraction.

to the substrate (*z* axis, as represented in Figure 4c). Such a preferential (or often uniaxial) contraction is well documented in the literature for mesostructured films exhibiting 2D-hexagonal mesostructure (*p*6*m*)[30,31,39,40] and has been recently described for a cubic *Im*3*m* mesophase.[70] For the *p*6*m* structure, the distorted hexagonal mesophase can be described as 2D-centered rectangular (*C*2*m*). The uniaxial contraction of the cubic *Im*3*m* mesostructure (Figure 3a) results in a high loss of symmetry. Formally, a triclinic unit cell can be found inside the distorted bcc mesostructure, but, for simplicity, the initial cubic lattice parameters, instead of those of the triclinic, will be used here to describe the structural changes along the treatment process.

SAXS data showed that the F127-templated $TiO_2$ cubic (or triclinic after contraction) mesostructure (Figure 9) is stable to temperatures higher than 600 °C. The (110) spots (the in-plane spots) become weak at 500 °C and above, which can be partially explained by the exponential decay of the reflection intensity for higher Bragg angles, but also by a reduction in the structural order along the direction parallel to the substrate (such planes are submitted to the highest degree of contraction). 2D-SAXS patterns collected in grazing incidence (see insets in Figure 9a) showed that the (110) spots are still present at 600 °C, although they are very weak. TEM images of 600 °C treated F127-templated films (Figure 10e and f) show that the cubic (or triclinic) mesostructure is fully preserved. The inorganic framework is still continuous, and the approximately 80 Å cagelike pores can be observed throughout the sample. These values are close to those reported for SBA-16 (cavities of 95 Å),[9,86] close to those reported for F127-templated cubic (*Im*3*m*) silica films (85 Å),[32] and the same as those reported for F127-templated trivalent metal-containing-zirconia (80 Å).[70] In fact, after contraction, the cagelike pores present themselves as ellipsoids of about 80 × 40 Å (for directions that are ∥ and ⊥ to the substrate, respectively). Such a high thermal stability for periodically organized mesoporous $TiO_2$ has never been reported. By 700 °C, only the (1-10) spots are still present in the SAXS patterns, indicating that the initial periodicity was retained only in the direction normal to the substrate. This loss of order can be seen by TEM (Figure 10i), which shows the growth of particles breaking up the continuity of the inorganic framework, but with a constant correlation distance in one direction; that is, the original cubic motif was partially preserved. Even though some of the order was lost, the porosity is still present at 700 °C, as one can see in Figure 10i.

For Brij-templated films, the stability is limited to 400 °C, as was previously described.[39] The lower thermal stability can be attributed to the smaller inorganic domains present in such films, as a result of the formation of smaller pores (and thus thinner walls for a similar $\Phi_T$), which cannot accommodate the crystallites formed at temperatures higher than 400 °C (see below). A similar effect has been reported for ABC-templated $ZrO_2$-based films.[77]

2D-hexagonal mesostructures present a lower thermal stability than the cubic mesostructures if templated by the same ABC. This can be attributed to the thinner inorganic walls. For example, the inorganic walls of a F127-templated 2D-hexagonal film are approximately 70 Å thick, while 100−120 Å walls can be observed for the cubic film (see Figures 5 and 10). The lower thermal stability of the 2D-hexagonal phase concerns mainly the periodicity, with the observation of a diffraction ring (characteristic of disordered domains) together with diffraction spots in the SAXS patterns of films calcined at 350 °C and above. By 450 °C, only a ring is still present. Even though the periodicity was lost by 450 °C, the porosity is still present at 600 °C (the highest temperature that was investigated for *p*6*m* structures).

**Crystallization of the Inorganic Framework.** For Pluronic-templated films, the crystallization of the inorganic framework starts by 350 °C with formation of anatase, as was previously described.[77] By 400 °C, few anatase crystallites of about 5 nm in diameter embedded in an amorphous matrix can be observed by HRTEM (Figure 10d, the crystallites are indicated by arrows), in excellent agreement with the size of the crystallites determined by XRD (see Figure 10a).[77] These results are similar to those reported by Alberius et al.[44] Further heating causes the growth of these crystallites, and, by 600 °C, crystallites of about 12 nm are observed by XRD, with anatase as the only present

(86) Sakamoto, Y.; Kaneda, M.; Terasaki, O.; Zhao, D. Y.; Kim, J. M.; Stucky, G.; Chin, H. J.; Ryoo, E. *Nature* **2000**, *408*, 449.

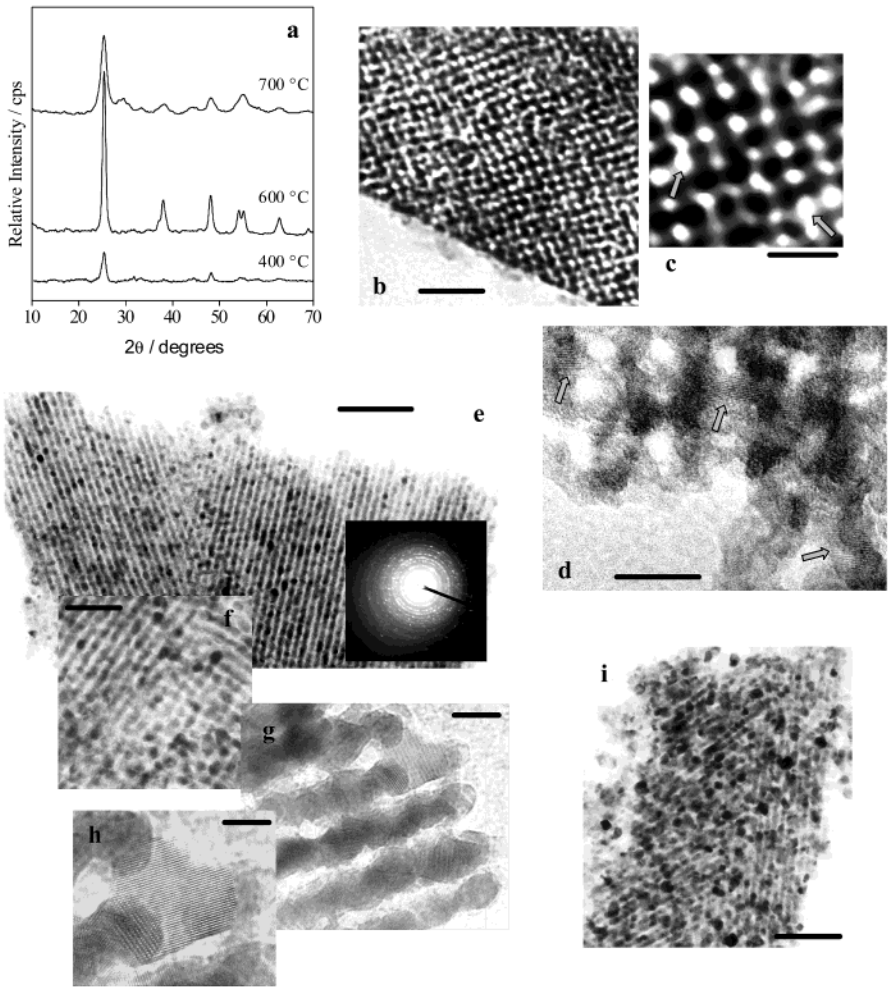


***Figure 10.*** (a) XRD patterns (parallel mode) of F127-templated $TiO_2$ films calcined at the temperatures indicated. TEM images of F127-templated cubic (*Im*3*m*) $TiO_2$ films: (b) and (c) 350 °C treated; (d) 400 °C (HRTEM) showing the presence of some anatase crystallites; (e−h) 600 °C treated, with increasing magnification to show from large areas of organized domains to the presence of anatase crystallites throughout the structure; the inset in part (e) is an ED pattern characteristic of anatase; (i) 700 °C treated sample. The images are cross sections perpendicular to the [111] (b and c), [100] (d and f), and [110] (e, g, h, and i) directions. Scale bars are (b) 50 nm, (c) 20 nm, (d) 10 nm, (e) 100 nm, (f) 50 nm, (g) 10 nm, (h) 5 nm, and (i) 100 nm.

phase (Figure 10a). HRTEM shows that, at this temperature, a practically fully crystallized inorganic framework is formed. In Figure 10g and h, the lattices fringes can be observed. In fact, by changing the focus in the same region, we could observe that these fringes are present throughout the structure.

By 700 °C, a phase transition from anatase to brookite takes place, as is revealed by XRD (Figure 10a). The broad peaks observed can be attributed to the superposition of various peaks of brookite, the structure of which is less symmetric than that of anatase. The stabilization of the anatase phase up to 600 °C and the transition to brookite (instead of rutile) can be attributed to the small size of inorganic domains. Zhang and Banfield[87] showed that the surface energy associated to the different phases of $TiO_2$ increases in the order anatase < brookite < rutile. Therefore, although rutile is the most stable phase for a bulk material, when a large amount of surface is present (such as for nanoparticles smaller than 14 nm), anatase is stabilized, minimizing the total free energy of the system (bulk + surface, see ref 73, p 47).

The key to the high stability of the cubic mesophase seems to be the presence of thick inorganic walls (clearly visualized in the center of each four pores square, particularly evident in Figures 5b and 10f). These approximately 100−120 Å domains can accommodate the crystallites formed in the 400−600 °C temperature range. For the 2D-hexagonal mesophase, the lower thermal stability (of the structural order) can be attributed to the presence of inorganic walls with thickness around 70 Å. Notably, the main degradation of such a mesostructure (2D) occurs together with the crystallite growth (350−450 °C, where polyoriented domains start to be observed). Therefore, the mesostructural degradation can be directly related to the formation of crystallites that exceed the size of the inorganic framework domains.[77]

In previous works, the authors underestimated the stability of the periodicity of F127-templated $TiO_2$ films to 400[39] or 500 °C.[77] This misunderstanding came from the use of XRD in $\theta-2\theta$ mode as the main technique for structural analysis. As a result, one can see that 2D-SAXS (or 2D-XRD) is the technique of choice to obtain structural information for these oriented mesostructured systems.

**Characteristics of the Coatings.** The film thickness, evaluated by ellipsometry (for details about the methods applied, see ref 39) and checked by SEM and TEM, can be adjusted in the

(87) Zhang, H.; Banfield, J. F. *J. Mater. Chem.* **1998**, *8*, 2073.

50−1000 nm range without cracking by varying dilution and deposition rate. Most of the analyses presented above were performed using films prepared using the optimal conditions described in the Experimental Section. In such conditions, the thickness of a calcined film lies in the 300−400 nm range. Such films are completely transparent in the 350−1100 nm range.

The surface area of these films varies according to $\Phi_T$ and pore size. Typically, the surface area of F127-templated films prepared applying the optimal conditions is around 150 $m^2\ g^{-1}$ [SI], lower than that of similar silica films. This result can be explained by the higher density of $TiO_2$ when compared to that of silica,[16] and a low amount of microporosity, evidenced by the small volume adsorbed at low pressure. Thus, the surface area mainly originates in the mesopores, unlike for PEO-based block copolymer templated silicas.[88] Indeed, this surface area is similar to that reported for a P123-templated $TiO_2$ powder, 205 $m^2\ g^{-1}$,[36] which was synthesized using a higher $\Phi_T$ than that prepared here. The isotherm is type IV, in which it is hard to identify the hysteresis loop as H1 or H2.[89] Usually, the $N_2$ adsorption isotherms of materials presenting a cagelike structure, such as the present *Im*3*m* symmetry, have a H2 hysteresis loop, associated to the presence of large pores connected by smaller openings (ink-bottle pores), typical of SBA-16[9] and also observed for F127-templated silica films.[32] Here, this effect seems to be minimized by the presence of defects in the pore walls, as one can see in Figure 10c (indicated by arrows). The average pore size around 58 Å is in very good agreement with the 40 × 80 Å cages observed by TEM.

**Investigation of the Chemical Events that Take Place during Film Formation, Stabilization, and Crystallization by EXAFS.** EXAFS experiments performed on the initial solutions were discussed in a preceding section. To summarize, in the absence of water, typical Ti−X (i.e., X is a first sphere neighbor) distances found were consistent with those of solvated Ti chloroalkoxide ($TiCl_2(EtO)_2$). The number of chloride neighbors decreases with increasing hydrolysis; at the same time, neighbors at shorter distances appear, which should correspond to hydroxo- or oxo- groups linked to Ti(IV) centers.

For the freshly deposited film, three distances are again found, but the longer Ti−O contribution now drops to 1.94 Å, a distance identical to the one observed in $TiO_2$−anatase (Table 1). This contribution clearly evidences the condensation of the titanium oxo-framework, in agreement with infrared ellipsometry [SI]. The third contribution corresponds to one chloride atom, still present in the titanium first neighbor shell at that stage of the process.

For the aged film, the same distances as those for the freshly deposited film are evidenced, but the number of long Ti−O (1.95 Å) bonds increases, indicating the progress of condensation. This increase is associated to a decrease of the Ti−Cl contribution (2.35 Å). For higher temperature processing, the Ti(IV) environment is quite similar to the one found in crystalline $TiO_2$ (vide supra).

All of these facts consolidate the image of a fresh film composed of small Ti-oxo-hydroxo oligomers, with some Cl atoms linked to titanium. The presence of Cl in the titanium coordination sphere likely favors the construction of Ti-oxo oligomers having lower $\mu$-oxo connectivity, allowing a better adjustment of the interfacial curvature. Moreover, these hydrophilic entities are gathered around a hybrid LC phase, thus forming a "titanotropic" mesostructured hybrid. The inorganic building blocks are weakly attached to one another (i.e., condensation is not extended), which imparts flexibility to the whole hybrid network. Upon heating, condensation is triggered, chloride terminal atoms are substituted by oxo bridges, HCl is eliminated (together with residual water and ethanol), and the inorganic network is strengthened; prolonged thermal treatment leads to a full crystalline mesoporous $TiO_2$.

## Conclusions

Mesoporous titania films have been prepared by dip-coating through evaporation-induced self-assembly, which associates the sol−gel method (with HCl as the condensation inhibitor) and the self-organization of amphiphilic block copolymers. The in situ analysis of the structural evolution related to the advancement of the evaporation process leads to an excellent comprehension of the role of each of the variables involved, allowing the reproducible formation of transparent, crack-free, and high surface area coatings, exhibiting different and tailored mesostructural symmetry (wormlike, cubic *Im*3*m*, 2D-hexagonal *p*6*m*). Crossing SAXS, XRD, and TEM analyses led to a complete characterization of the mesostructure and its alignment to the substrate, while IR, $^{17}O$ NMR, and EXAFS allow one to identify the important chemical features involved in the processes leading from the solution to the hybrid solids.

The most important events in the formation of ordered mesoporous $TiO_2$ films are summarized in Scheme 1. The reaction of $TiCl_4$ with ethanol produces, as was previously described and checked here by EXAFS and UV−vis experiments, metallic chloroethoxide precursors [$TiCl_{4-x}(OEt)_x$], with $x \approx 2$.[47,90] To this highly acidic system could be added water in controlled quantities. Once $h > 4$, the final solutions contain hydrolyzed hydrophilic moieties,[73] which are predominantly $\mu_2$-O-bridged dimers, as was revealed by $^{17}O$ NMR and EXAFS. UV−vis and EXAFS data also showed that these species contain a certain quantity of Ti−Cl bonds, the six-fold coordination sphere of Ti being completed by OH and $H_2O$.

During dip-coating, a fast evaporation of EtOH is observed, accompanied by HCl and $H_2O$. Besides, MS, EDX, and Karl Fisher results showed that $H_2O$ and HCl progressively concentrate in the coating during evaporation of this EtOH-rich mixture. When the drying line is reached, the film is in a modulable steady state that can be modified by the environment. At this stage, the humidity in the atmosphere is a crucial parameter. Karl Fisher and ellipsometry results showed that the water content in the coating can be as low as 3% (at RH < 10%) or as high as 50% (at RH > 70%). This water content determines the fluidity of the deposited coating and thus the possibility of the occurrence of the disorder-to-order transition. Moreover, the water content can control the final mesophase, because it affects the inorganic volume.[34,70] An appropriate sequence of posttreatments in dry/wet atmosphere can be used to optimize the film texturation, while attaining an excellent optical quality.[70]

(88) Impéror-Clerc, M.; Davidson, P.; Davidson, A. *J. Am. Chem. Soc.* **2000**, *122*, 11925. (b) Ryoo, R.; Ko, C. H.; Kruk, M.; Antochshuk, V.; Jaroniec, M. *J. Phys. Chem. B* **2000**, *104*, 11465.
(89) Kruk, M.; Jaroniec, M. *Chem. Mater.* **2001**, *13*, 3169.
(90) Nabavi, M.; Doeuff, S.; Sanchez, C.; Livage, J. *J. Non-Cryst. Solids* **1990**, *121*, 31.

***Scheme 1.*** Sequential Events in the Formation of Ordered Mesoporous $TiO_2$ Films

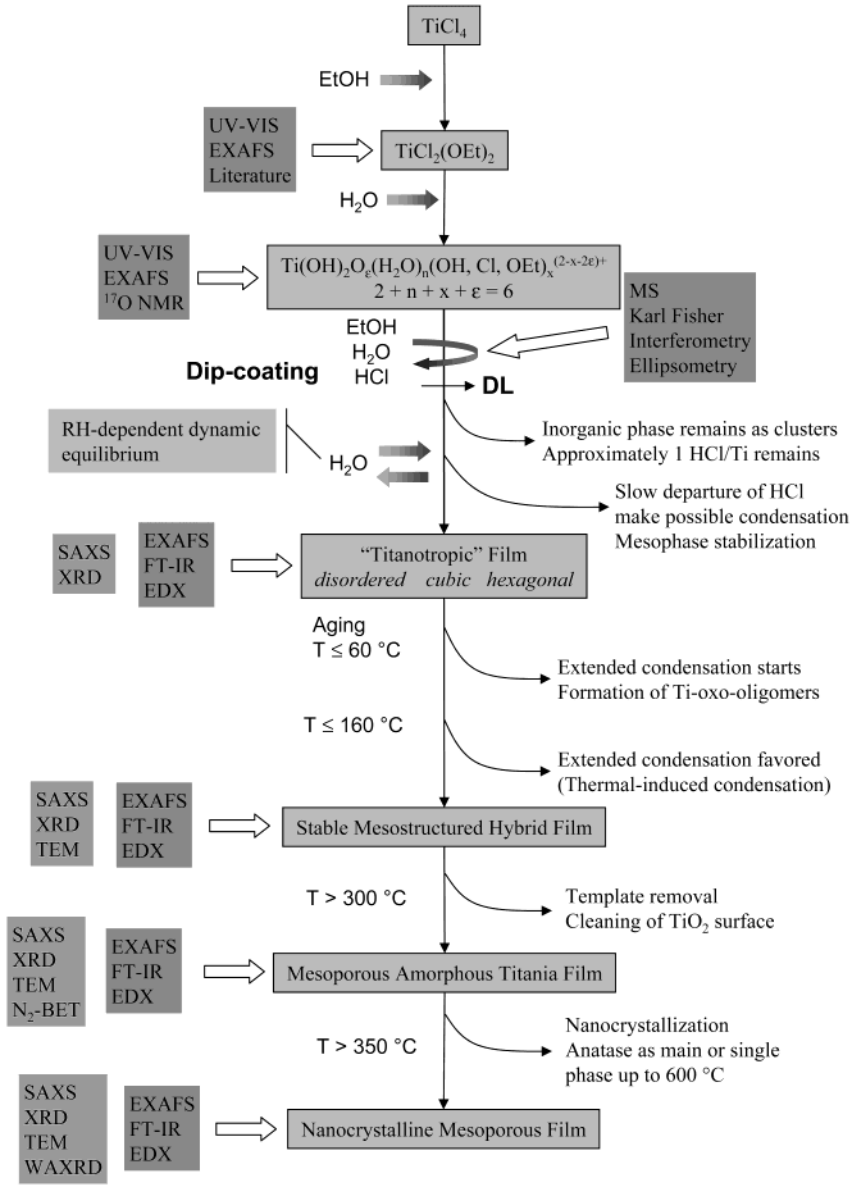


Once the mesophase is formed, its stabilization is possible due to the slow departure of residual HCl (at this stage, approximately 1Cl/Ti remains in the coating, which limits extended condensation). Extended condensation is then acquired by heating the film between 60 and 160 °C, as was observed by EXAFS and FT-IR. The way chosen to carry out this sequence of treatments is very important for the stability of the mesostructure. Slow elimination of the volatile species (water, HCl) favors the formation of a more cross-linked $TiO_2$ framework, which contracts less and is more thermally stable after template removal.

Template-free mesoporous films are obtained at temperatures higher than 300 °C. At 350 °C, the coatings start to crystallize, with the formation of anatase as the main phase up to 600 °C. Treatment at temperatures between 400 and 600 °C give rise to high surface area mesoporous nanoanatase coatings.

In addition, the understanding of the processes brought by this work has allowed us to extend these preparation methods to the formation of submicrometric mesoporous (or meso/macroporous) spherical particles by aerosol, opening new opportunities for the design of shape-tailored nanoporous materials.[91]

**Acknowledgment.** This work was financially supported by the French Ministry of Research, CNRS, CNPq (Brazil, grant no. 200636/00-0), and Fundación Antorchas (Argentina Project# 13956-74, and RG 14056-18). The authors thank Dr. Pierre-Antoine Albouy, Dr. Heinz Amenistch, and Dr. Dominique Durand for help with synchrotron-SAXS measurements. The authors also thank J. A. Maulin and M. T. P. Maglia, and the Laboratório de Microscopia Eletrônica of the Depto. de Biologia Celular Molecular e Bioagentes Patogênicos, Faculdade de Medicina de Ribeirão Preto, University of São Paulo, and Fabienne Warmont (Univ Paris VI) for the TEM pictures. F. Villain is acknowledged for her

(91) Grosso, D.; Soler-Illia, G. J. de A. A.; Crepaldi, E. L.; Charleaux, B.; Sanchez, C. *Adv. Funct. Mater.* **2003**, *13*, 37.

assistance in the EXAFS measurements. The authors are deeply indebted to A. Brunet-Bruneau and A. Bourgeois for the ellipsometry measurements, and to J. Blanchard for the access to MS.

**Supporting Information Available:** Characterization data and figures (PDF). This material is available free of charge via the Internet at http://pubs.acs.org.

JA030070G